Article

Bacterial inhibition of Fas-mediated killing promotes neuroinvasion and persistence

https://doi.org/10.1038/s41586-022-04505-7

Received: 20 November 2020

Accepted: 3 February 2022

Published online: 16 March 2022

Check for updates

Claire Maudet[1,5], Marouane Kheloufi[1,5], Sylvain Levallois[1], Julien Gaillard[1], Lei Huang[1], Charlotte Gaultier[1], Yu-Huan Tsai[1,4], Olivier Disson[1] & Marc Lecuit[1,2,3] ✉

Infections of the central nervous system are among the most serious infections[1,2], but the mechanisms by which pathogens access the brain remain poorly understood. The model microorganism *Listeria monocytogenes* (*Lm*) is a major foodborne pathogen that causes neurolisteriosis, one of the deadliest infections of the central nervous system[3,4]. Although immunosuppression is a well-established host risk factor for neurolisteriosis[3,5], little is known about the bacterial factors that underlie the neuroinvasion of *Lm*. Here we develop a clinically relevant experimental model of neurolisteriosis, using hypervirulent neuroinvasive strains[6] inoculated in a humanized mouse model of infection[7], and we show that the bacterial surface protein InlB protects infected monocytes from Fas-mediated cell death by $CD8^+$ T cells in a manner that depends on c-Met, PI3 kinase and FLIP. This blockade of specific anti-*Lm* cellular immune killing lengthens the lifespan of infected monocytes, and thereby favours the transfer of *Lm* from infected monocytes to the brain. The intracellular niche that is created by InlB-mediated cell-autonomous immune resistance also promotes *Lm* faecal shedding, which accounts for the selection of InlB as a core virulence gene of *Lm*. We have uncovered a specific mechanism by which a bacterial pathogen confers an increased lifespan to the cells it infects by rendering them resistant to cell-mediated immunity. This promotes the persistence of *Lm* within the host, its dissemination to the central nervous system and its transmission.

The factors of *Listeria monocytogenes* (*Lm*) that promote its neuroinvasion, and their mechanisms of action, are poorly understood. Previous studies have suggested that monocytes are involved in transferring *Lm* from the blood to the central nervous system (CNS)[8,9]. However, these investigations were performed with poorly neuroinvasive[6] reference laboratory *Lm* strains, which require very high bacterial inocula to induce infection of the CNS in experimental animal models. This is consistent with the observation that these strains belong to clonal complexes that are very rarely responsible for human neurolisteriosis[3,6]. By contrast, clinically associated clonal complexes are hypervirulent and more neuroinvasive[6]. To investigate the mechanisms that underlie *Lm* neuroinvasion, here we developed a clinically relevant experimental model of neurolisteriosis that is based on the inoculation of hypervirulent neuroinvasive *Lm* strains[6] in a humanized mouse model[7].

Monocytes mediate *Lm* neuroinvasion

We orally inoculated *Lm* in humanized KIE16P mice, which are permissive to orally acquired listeriosis[7]. In contrast to the reference strain EGDe, which belongs to the clonal complex (CC) 9 (refs. [10,11]), clinical isolates that belong to the hypervirulent clonal complexes CC1, CC4 and CC6 systematically induce high-level neuroinvasion, as previously reported[6], starting at 3 days post-inoculation (dpi) (Fig. 1a). At 5 dpi, the bacterial load in the brain is the same with or without administration of gentamicin (Fig. 1b, Extended Data Fig. 1a), an antibiotic that kills extracellular (Extended Data Fig. 1b) but not intracellular *Lm* (ref. [12]), indicating that intracellular bacteria are involved in neuroinvasion. Consistently, neuroinvasive *Lm* are detected in the blood (Extended Data Fig. 1c), and are predominantly found in inflammatory monocytes ($CD45^+CD11b^+Ly6C^+CD3^-CD19^-CD11c^-Ly6G^-$) in the blood and spleen (Fig. 1c, d, Extended Data Fig. 1d, e), which suggests that monocytes are involved in *Lm* neuroinvasion. This was confirmed by infecting $Ccr2^{-/-}$ mice, in which monocytes are retained in the bone marrow and are therefore less abundant in the blood and spleen[13] (Extended Data Fig. 1f). Indeed, from 1–3 dpi, more bacteria are gradually recovered from the brain of wild-type mice as compared to $Ccr2^{-/-}$ mice (Fig. 1e). Moreover, the transfer of infected monocytes from donor-infected mice into gentamicin-treated uninfected recipient mice (Extended Data Fig. 1g) is sufficient to induce neuroinvasion as early as day 2 after transfer (Fig. 1f). By contrast, the transfer of infected monocytes from mice expressing the diphtheria toxin receptor in myeloid cells (*LysM*-$CreER^{T2}$ × iDTR) into recipient mice treated with diphtheria toxin to deplete transferred monocytes leads to liver and spleen infection but no brain infection, even as late as four days after transfer (Extended Data Fig. 1h, i). Together, these results indicate that infected monocytes are necessary and sufficient to induce neuroinvasion.

[1]Institut Pasteur, Université de Paris, Inserm U1117, Biology of Infection Unit, Paris, France. [2]Institut Pasteur, National Reference Center and WHO Collaborating Center Listeria, Paris, France. [3]Necker-Enfants Malades University Hospital, Division of Infectious Diseases and Tropical Medicine, APHP, Institut Imagine, Paris, France. [4]Present address: Institute of Microbiology and Immunology, National Yang-Ming University, Taipei, Taiwan. [5]These authors contributed equally: Claire Maudet, Marouane Kheloufi. ✉e-mail: marc.lecuit@pasteur.fr

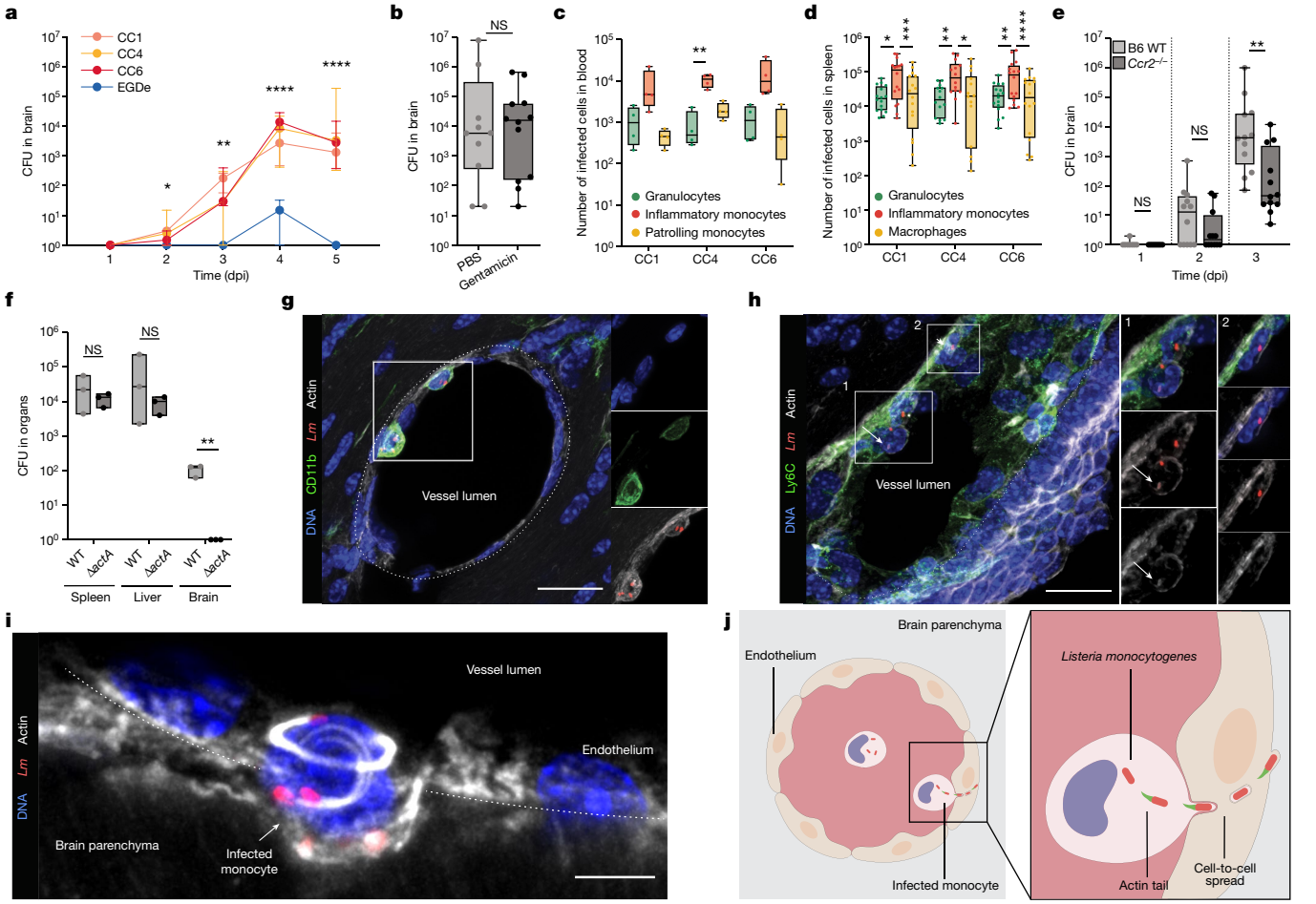

Fig. 1 | Infected inflammatory monocytes transfer *Lm* to the CNS by cell-to-cell spread. a, Bacterial load in the brain of mice after inoculation with the *Lm* strains CC1, CC4, CC6 or EGDe (oral, 2×10^8 colony-forming units (CFU)). **b**, Bacterial load in the brain of gentamicin-treated mice five days after inoculation with CC4 *Lm* (oral, 2×10^8 CFU). **c**, **d**, Three of the main infected cell populations in the blood (**c**) and spleen (**d**) of mice after inoculation with CC1, CC4 or CC6 *Lm* (oral, 2×10^8 CFU), at 4 dpi, the peak of bacteraemia (related to Extended Data Fig. 1c). For the blood, three mice are pooled together for each dot. **e**, Bacterial load in the brain of B6 wild-type (WT) and *Ccr2*$^{-/-}$ mice after inoculation with CC4 *Lm* (intravenous, 1×10^4 CFU). **f**, Bacterial load of gentamicin-treated recipient mice, two days after injection of infected monocytes collected from six donor mice that were infected for three days with either wild-type CC4 or CC4Δ*actA* (intravenous, 1×10^4 CFU). **g**–**i**, Representative immunofluorescence images of infected monocytes adhering to endothelial cells (**g**); monocytes infected by an actin-polymerizing *Lm* (arrow) adjacent to an infected endothelial cell (arrowhead) (**h**) and an adhering infected monocyte (arrowhead) with actin comet-tails (**i**) two days after inoculation with CC1 *Lm* (intravenous, 5×10^5 CFU (**g**, **h**)) or CC4 *Lm* (intravenous, 5×10^5 CFU (**i**)). Scale bars, 20 µm (**g**, **h**); 5 µm (**i**). Maximum intensity projection over an 8-µm stack (**g**–**i**). Insets are single *z*-planes (**h**). **j**, Schematic representation of the *Lm* neuroinvasion process. $^*P < 0.05$, $^{**}P < 0.01$, $^{***}P < 0.001$, $^{****}P < 0.0001$; NS, not significant ($P > 0.05$); see the 'Statistical analysis' section for statistical tests.

Infected monocytes are observed adhering to the endothelium of blood vessels in brain sections of infected mice (Fig. 1g, h, Extended Data Fig. 1j–l). In these adhering monocytes, actin-polymerizing *Lm* are observed—significantly more than in spleen monocytes, and occasionally adjacent to infected endothelial cells (Fig. 1h, i, Extended Data Fig. 1m–p, Supplementary Videos 1–3). Moreover, the transfer of monocytes infected with an *Lm*Δ*actA* isogenic mutant, which is unable to polymerize actin and mediate cell-to-cell spread[14,15], does not induce neuroinvasion—in contrast to the transfer of monocytes infected with wild-type *Lm* to the same level (Fig. 1f, Extended Data Fig. 1g). Together, these results show that *Lm* accesses the brain parenchyma by actin assembly–inducing protein (ActA)-mediated cell-to-cell spreading from adhering bloodborne infected inflammatory monocytes (Fig. 1j). These results are in line with previous reports that were obtained using poorly neuroinvasive *Lm* strains[8,9], and suggest that neuroinvasive *Lm* strains invade the CNS in a similar manner, albeit to a far greater efficiency (up to three orders of magnitude) (Fig. 1a).

InlB promotes *Lm* neuroinvasion

Having identified infected monocytes as being critically involved in the onset of neurolisteriosis, we looked for factors in *Lm* that mediate its neuroinvasiveness. Given the well-established roles of InlA and InlB in the crossing of intestinal barriers[16] and placental barriers[7] by *Lm*, we investigated their roles in neuroinvasion. To bypass the contribution of InlA in the crossing of the intestinal barrier, we inoculated KIE16P mice by the intravenous route. Although InlA is not involved in neuroinvasion, InlB has a major role: the Δ*inlB* mutant is significantly less neuroinvasive than its wild-type parental strain in co-infection experiments (Fig. 2a, b, Extended Data Fig. 2a–e). Accordingly, the Δ*inlAB* mutant (in which both *inlA* and *inlB* are deleted) is no less neuroinvasive than the Δ*inlB* mutant (Extended Data Fig. 2f, g), thus ruling out the possibility that InlA has any effect on neuroinvasion. After oral inoculation, a similar difference in neuroinvasiveness is observed between all representative wild-type strains of neuroinvasive clones and their corresponding Δ*inlB* mutant (Fig. 2c,

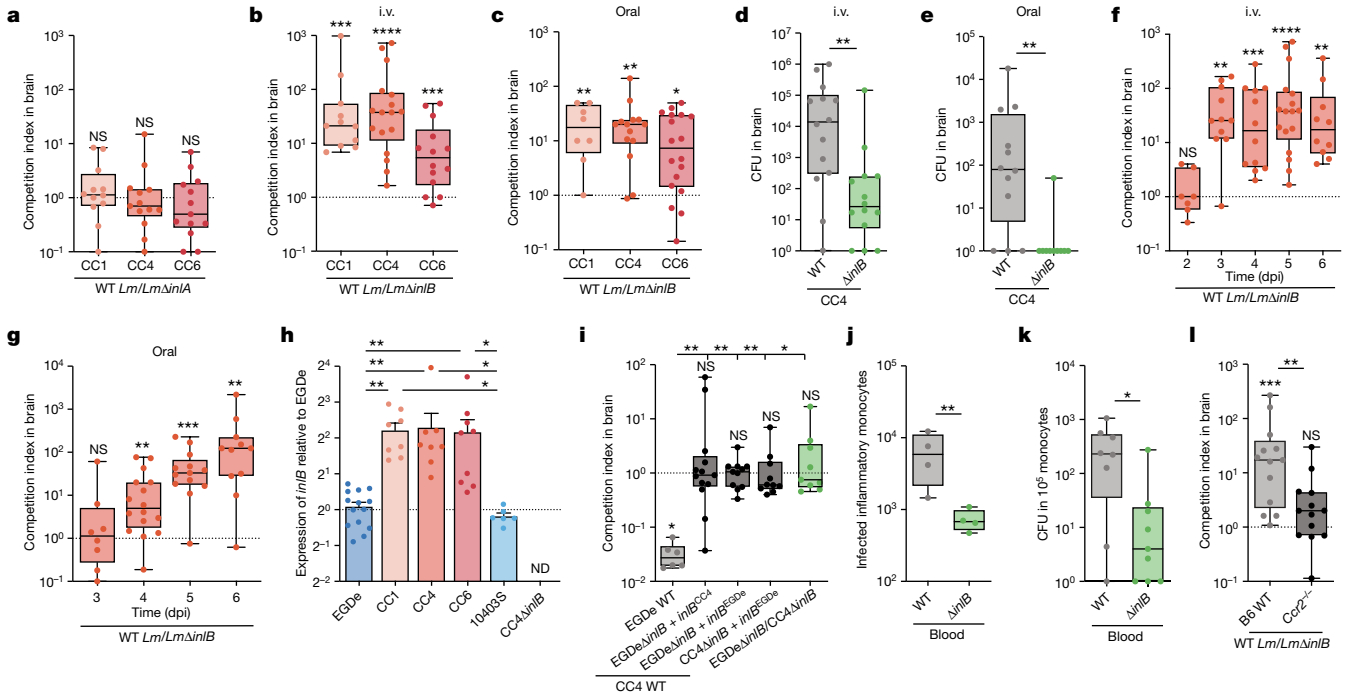

Fig. 2 | InlB is involved in *Lm* neuroinvasion and increases the infection of inflammatory monocytes. a–**c**, Competition indexes in the brain five days after inoculation with a 1:1 mix of *Lm* wild-type and isogenic mutant strains. **a**, Wild-type *Lm* and *LmΔinlA* (intravenous, 1×10^4 CFU). **b**, **c**, Wild-type *Lm* and *LmΔinlB* (intravenous (i.v.), 1×10^4 CFU (**b**); oral, 2×10^8 CFU (**c**)). **d**, **e**, Bacterial load in the brain after inoculation with either wild-type CC4 or CC4Δ*inlB* (intravenous, 1×10^4 CFU (**d**); oral, 2×10^8 CFU (**e**)), at 4 dpi (**d**) or 5 dpi (**e**). **f**, **g**, Competition indexes in the brain after inoculation with a 1:1 mix of wild-type CC4 and CC4Δ*inlB* (intravenous, 1×10^4 CFU (**f**); oral, 2×10^8 CFU (**g**)). **h**, Transcription levels of *inlB* relative to EGDe in infected splenocytes in vivo two days after intravenous inoculation. ND, not detected. **i**, Competition index in the brain five days after inoculation with a 1:1 mix of the indicated bacterial strains (intravenous, 2×10^4 CFU for EGDeΔ*inlB*/CC4Δ*inlB* and 1×10^4 CFU for all others). **j**, **k**, Number of infected monocytes (**j**) and bacterial enumeration from sorted total (uninfected + infected) monocytes (**k**) in the blood four days after inoculation with wild-type CC4 or CC4Δ*inlB* (oral; 2×10^8 CFU (**j**); intravenous, 1×10^4 CFU (**k**)). **l**, Competition index in the brain of control or *Ccr2*$^{-/-}$ mice three days after inoculation with a 1:1 mix of wild-type CC4 and CC4Δ*inlB* (intravenous, 1×10^4 CFU). $^*P < 0.05$, $^{**}P < 0.01$, $^{***}P < 0.001$, $^{****}P < 0.0001$; NS, not significant ($P > 0.05$); see the 'Statistical analysis' section for statistical tests. CFU data corresponding to competition indexes are shown in Extended Data Figs. 2, 3.

Extended Data Fig. 2h). The involvement of InlB in neuroinvasion is also observed after separate inoculation with either wild-type *Lm* or *LmΔinlB* (Fig. 2d, e, Extended Data Fig. 2i, j). The contribution of InlB to neuroinvasion starts at day 3 and day 4 after intravenous and oral inoculation, respectively, and increases over time, and *LmΔinlB* never reaches the levels of wild-type *Lm* in terms of infection in the brain (Fig. 2f, g, Extended Data Fig. 2k, l).

The critical role of *inlB* in *Lm* neuroinvasion is notable as this gene is part of the *Lm* core genome and is therefore present in all *Lm* strains[17], including the poorly neuroinvasive reference strains EGDe and 10403S. Neuroinvasive *Lm* isolates actually strongly upregulate the *inlAB* operon as compared to EGDe and 10403S, both in vitro in liquid medium and in vivo in infected spleen (Fig 2h, Extended Data Fig. 2m–p). These results, together with the observation that EGDe neuroinvasion—although extremely low compared to CC4 (Fig 1a)—also depends on InlB (Extended Data Fig. 2q), suggest that the neuroinvasiveness of *Lm* requires that InlB is highly expressed. To test this, we complemented the EGDeΔ*inlB* mutant with the *inlB* gene sequence from either EGDe or CC4 (whose primary sequences are 93% identical; Supplementary Table 1) in such a way that the *inlB* within-host transcription levels are similar to those of endogenous *inlB* in CC4 (Extended Data Fig. 2r). These complemented strains become as neuroinvasive as wild-type CC4, whereas CC4Δ*inlB* is as poorly neuroinvasive as EGDeΔ*inlB* (Fig. 2i, Extended Data Fig. 2s, t). Consistently, CC4Δ*inlB* complemented with the *inlB* allele of EGDe and expressed to the level of CC4 in vivo is as neuroinvasive as wild-type CC4 (Fig. 2i, Extended Data Fig. 2s). Altogether, these results establish that overexpression of InlB is critical for *Lm* neuroinvasiveness.

We next evaluated the contribution of InlB to the infection of inflammatory monocytes, which are essential to *Lm* neuroinvasion (Fig. 1). From 3 dpi, the blood bacterial load is higher for wild-type *Lm* than for *LmΔinlB* (Extended Data Fig. 3a, b). Moreover, InlB significantly increases the number of *Lm*-infected inflammatory monocytes in the blood and spleen, but not the number of bacteria per infected monocyte (Fig. 2j, k, Extended Data Fig. 3c–f). Mice infected with the EGDe strain, which expresses InlB at a significant lower level than CC4, also exhibit a lower number of infected monocytes (Extended Data Fig. 3g). In addition, wild-type *Lm* is as poorly neuroinvasive as *LmΔinlB* in *Ccr2*$^{-/-}$ mice (Fig. 2l, Extended Data Fig. 3h), indicating that the contribution of InlB to neuroinvasion implicates infected monocytes. At early time points, when equal numbers of wild-type and Δ*inlB* bacteria are retrieved from the blood and brain, equivalent numbers of wild-type- and Δ*inlB*-infected adhering monocytes are also observed in the brain (1–2 dpi; Extended Data Figs. 1l, 3i, j), demonstrating that InlB has no effect on the ability of monocytes to adhere to brain vessels. Moreover, no effect of InlB on bacterial growth is detected after direct inoculation of *Lm* into the brain (Extended Data Fig. 3k, l). Together, these results indicate that InlB mediates neuroinvasion by increasing the number of circulating infected monocytes, which are themselves required for *Lm* neuroinvasion.

InlB has been described as an invasion protein that mediates the internalization of *Lm* into non-phagocytic cells[18–20]. However, the entry of hypervirulent *Lm* into inflammatory monocytes—which are professional phagocytes—is InlB-independent (Extended Data Fig. 3m–o). This indicates that the contribution of InlB to neuroinvasion is independent of its capacity to induce internalization; and indeed, InlB does

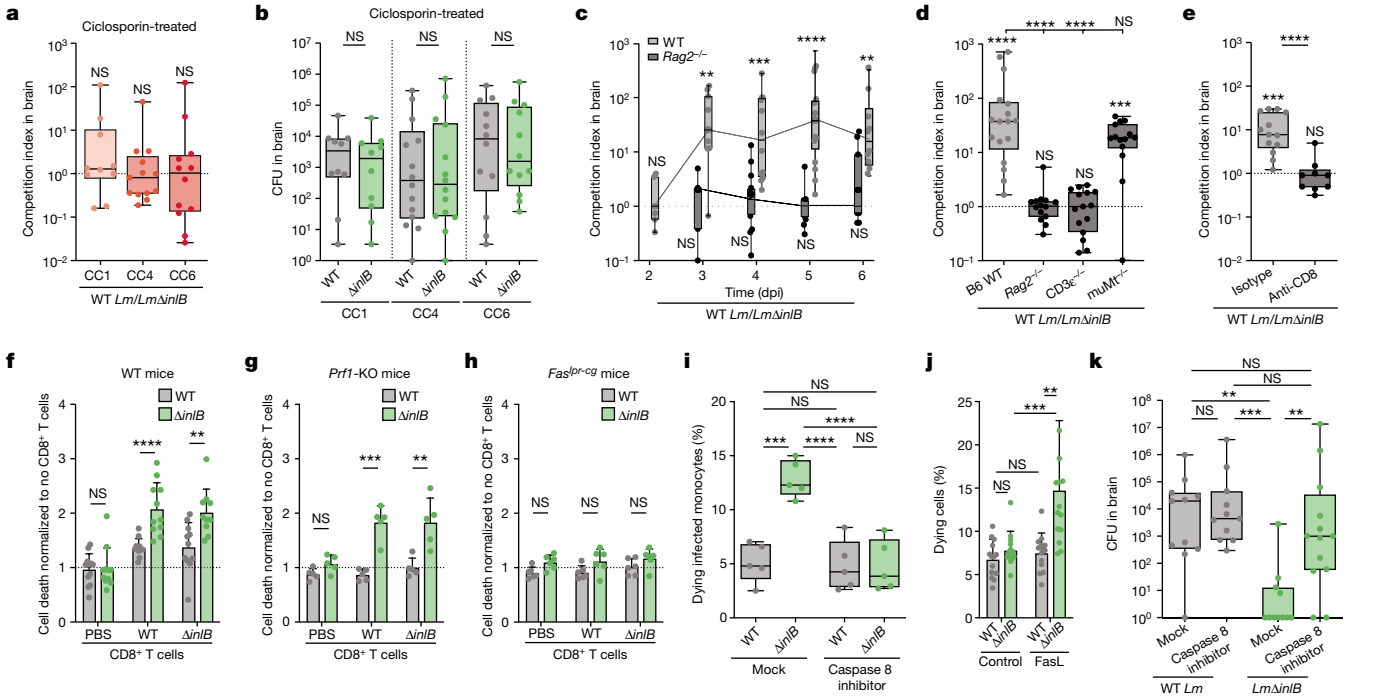

Fig. 3 | InlB blocks the CD8$^+$ T cell-mediated cell death of monocytes. **a**, **b**, Competition index (**a**) and bacterial load (**b**) in the brain five days after inoculation with a 1:1 mix of *Lm* wild-type and *Lm*Δ*inlB* isogenic mutant strains (oral, 5×10^7 CFU) in ciclosporin-treated mice (related to Fig. 2c, Extended Data Fig. 2h). **c**, Competition index in the brain after inoculation with a 1:1 mix of wild-type CC4 and CC4Δ*inlB* (intravenous, 1×10^4 CFU) in control and *Rag2*$^{-/-}$ mice. **d**, Competition index in the brain five days after inoculation with a 1:1 mix of wild-type CC4 and CC4Δ*inlB* (intravenous, 1×10^4 CFU) in B6 wild-type mice and in mice lacking functional T lymphocytes (CD3ε$^{-/-}$), B lymphocytes (muMt$^{-/-}$) or both (*Rag2*$^{-/-}$). **e**, Competition index in the brain five days after inoculation (oral, 2×10^8 CFU) with a 1:1 mix of wild-type CC4 and CC4Δ*inlB* after depletion of CD8$^+$ T cells. **f**–**h**, Level of caspase-3 cleavage in infected spleen monocytes collected from wild-type (**f**), *Prf1* knockout (KO) (**g**) or *Fas*$^{lpr\text{-}cg}$ (**h**) mice three days after inoculation with wild-type CC4 or CC4Δ*inlB* (intravenous, 1×10^4 CFU) and incubated with CD8$^+$ T cells from similarly infected (wild-type or Δ*inlB*) or control (PBS) mice at an effector-to-target ratio of 5. **i**, Proportion of dying (Zombie-positive) infected spleen monocytes three days after inoculation with wild-type CC4 or CC4Δ*inlB* (intravenous, 1×10^4 CFU) in mice treated with caspase-8 inhibitor. **j**, Level of caspase-3 cleavage in infected spleen monocytes collected three days after inoculation with wild-type CC4 or CC4Δ*inlB* (intravenous, 1×10^4 CFU) and treated ex vivo with FasL. **k**, Bacterial load in the brain five days after inoculation with wild-type CC4 or CC4Δ*inlB* (oral, 2×10^8 CFU) in mice treated with caspase-8 inhibitor. *$P < 0.05$, **$P < 0.01$, ***$P < 0.001$, ****$P < 0.0001$; NS, not significant ($P > 0.05$); see the 'Statistical analysis' section for statistical tests. CFU data corresponding to competition indexes are shown in Extended Data Figs. 2, 4 6.

not increase the number of bacteria per infected monocyte (Extended Data Fig. 3f). We therefore investigated how InlB could lead to a higher number of infected monocytes.

InlB prevents killing by CD8$^+$ T cells

T cell immunosuppression is a well-established risk factor for neurolisteriosis[3,21,22], and hypervirulent *Lm* clones that overexpress InlB (Fig. 2h) tend to infect individuals who are the least immunosuppressed[6]. This led us to hypothesize that InlB exhibits immunosuppressive properties. Treatment with ciclosporin, a prototypic T cell immunosuppressant, increases neuroinvasion and renders it independent of InlB (compare Fig. 3a with Fig. 2c, and Fig. 3b with Extended Data Fig. 2h), highlighting that the contribution of InlB to neuroinvasion is detectable only when adaptive immune responses are functional. Consistently, no difference in neuroinvasion is observed between wild-type *Lm* and *Lm*Δ*inlB* before 3 dpi (Fig. 2f, g, Extended Data Fig. 2k, l), when adaptive immune responses are not yet expected to be active[23]. Of note, treating EGDe-inoculated mice with ciclosporin leads to a slight increase in the number of infected inflammatory monocytes, and increases neuroinvasion, which also becomes independent of InlB (Extended Data Fig. 4a–e). As in ciclosporin-treated mice, *Lm* neuroinvasion is increased in *Rag2*$^{-/-}$ mice that lack T and B lymphocytes, and is fully InlB-independent (Fig. 3c, Extended Data Figs. 2k, 4d–h), indicating that the contribution of InlB to neuroinvasion requires functional lymphocytes. InlB-mediated neuroinvasion is abrogated in CD3ε$^{-/-}$ but not in muMt$^{-/-}$ mice (Fig. 3d, Extended Data Fig. 4i–k), indicating that it depends on T but not on B lymphocytes. Indeed, depletion of CD8$^+$ T cells increases *Lm* neuroinvasion and fully abrogates the contribution of InlB to neuroinvasion (Fig. 3e, Extended Data Fig. 4l, m). Notably, specific anti-*Lm* CD8$^+$ T cells are induced and activated to the same extent by wild-type *Lm* and its *Lm*Δ*inlB* isogenic mutant (Extended Data Fig. 5a–j), and mice inoculated with wild-type *Lm* or *Lm*Δ*inlB* promote the same level of protective immunity after a second challenge (Extended Data Fig. 5k). As *Lm* neuroinvasion is increased in the absence of functional CD8$^+$ T cells, becomes InlB-independent in the absence of functional CD8$^+$ T cells, relies on infected monocytes and is detectable in co-infection experiments, we reasoned that InlB may protect specifically infected monocytes from anti-*Lm*-specific killing by CD8$^+$ T cells. We therefore performed cytotoxic T lymphocyte (CTL) assays (Extended Data Fig. 5l). In sharp contrast to *Lm*Δ*inlB*-infected monocytes, monocytes infected with wild-type *Lm* are protected from CD8$^+$ T cell-mediated cell death (Fig. 3f, Extended Data Fig. 5m, n). Of note, the cytotoxicity mediated by CD8$^+$ T cells from either wild-type *Lm* or *Lm*Δ*inlB* infected mice is similar (Fig. 3f), confirming that InlB has no effect on *Lm* immunizing capacity (Extended Data Fig. 5a–k). In vivo, splenic *Lm*Δ*inlB*-infected monocytes also die twice more than monocytes infected with wild-type *Lm* (Fig. 3i). The observations that first, association of InlB with the bacterial surface is required for InlB-mediated neuroinvasion; second, infection of monocytes is clonal; and third, the contribution of InlB to neuroinvasion is detectable in co-infection experiments (Extended Data Fig. 6a–e) fully support the conclusion that InlB acts in a cell-autonomous manner.

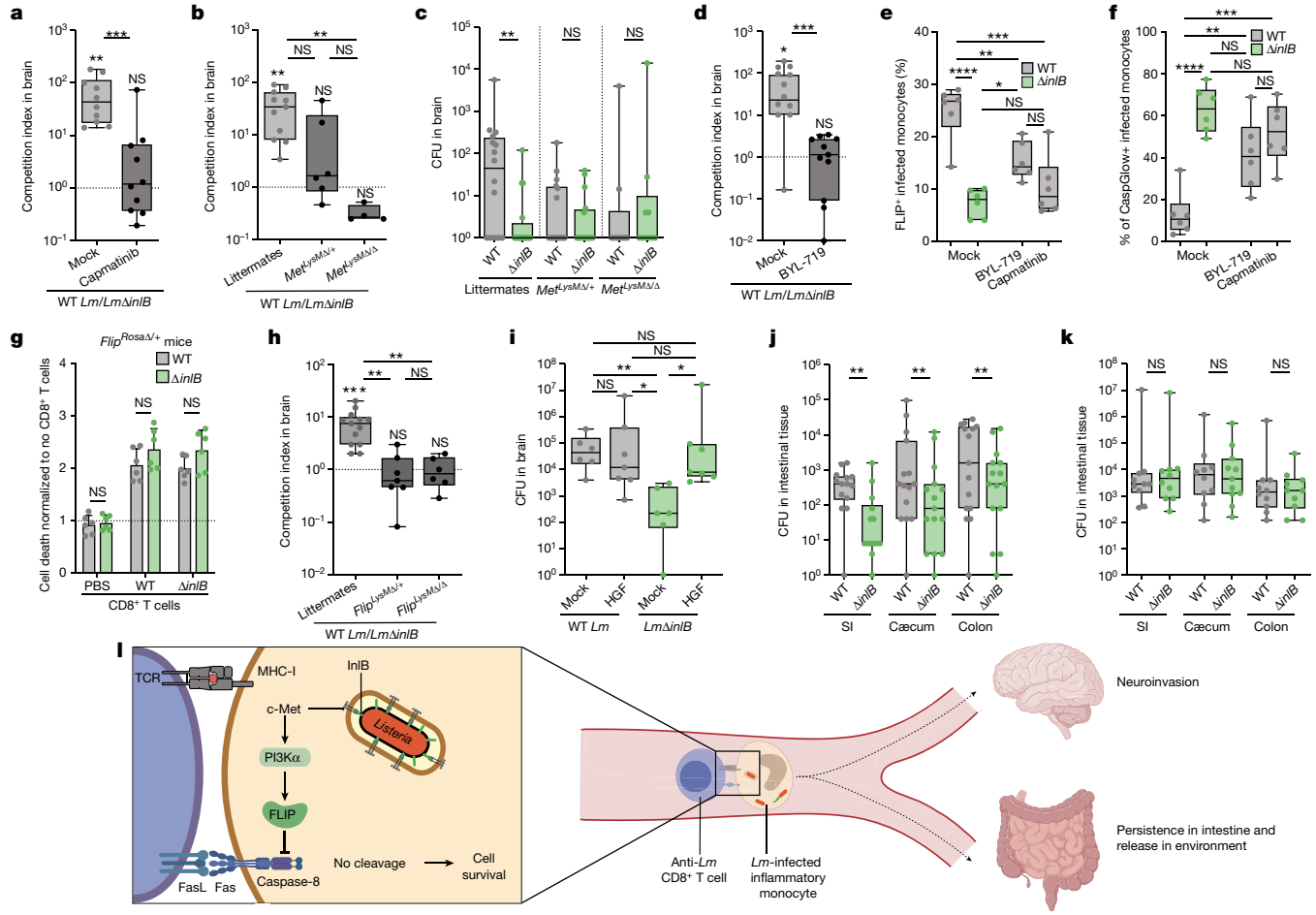

Fig. 4 | InlB blocks CD8$^+$ T cell-mediated killing through c-Met–PI3K–FLIP, and favours the persistence of *Lm* in the gut. a, Competition indexes in the brain five days after inoculation with a 1:1 mix of wild-type CC4 and CC4Δ*inlB* (oral, 2×10^8 CFU), in mice treated with a c-Met inhibitor (capmatinib). **b**, **c**, Competition index (**b**) and bacterial load (**c**) in the brain of tamoxifen-treated *LysM*-CreER^{T2} × *Met*$^{flox/flox}$ (and *LysM*-CreER^{T2} × *Met*$^{+/flox}$) mice (referred to as *Met*$^{LysMΔ/Δ}$ and *Met*$^{LysMΔ/+}$ mice), and their littermates, five days after inoculation with a 1:1 mix of wild-type CC4 and CC4Δ*inlB* (intravenous, 1×10^4 CFU). **d**, Competition index in the brain five days after inoculation with a 1:1 mix of wild-type CC4 and CC4Δ*inlB* (oral, 2×10^8 CFU), in mice treated with a specific PI3Kα inhibitor (BYL-719). **e**, **f**, Proportion of infected monocytes expressing FLIP (**e**) or active caspase-8 (**f**) three days after inoculation with wild-type CC4 or CC4Δ*inlB* (intravenous, 1×10^4 CFU) in mice treated with either BYL-719 or capmatinib. **g**, Level of caspase-3 cleavage in infected spleen monocytes, collected from tamoxifen-treated *Rosa26*-CreER^{T2} × *Cflar*$^{+/flox}$ (*Flip*$^{RosaΔ/+}$) mice three days after inoculation with wild-type CC4 or CC4Δ*inlB* (intravenous, 1×10^4 CFU) and incubated with CD8$^+$ T cells from similarly infected mice at an effector-to-target ratio of 5. **h**, Competition index in tamoxifen-treated *LysM*-CreER^{T2} × *Flip*$^{flox/flox}$ (or *LysM*-CreER^{T2} × *Flip*$^{+/flox}$) mice (referred to as *Flip*$^{LysMΔ/Δ}$ and *Flip*$^{LysMΔ/+}$ mice), and their littermates, five days after inoculation with a 1:1 mix of wild-type CC4 and CC4Δ*inlB* (intravenous, 1×10^4 CFU). **i**, Bacterial load in the brain five days after inoculation with either wild-type CC4 or CC4Δ*inlB* (intravenous, 1×10^4 CFU) in mice treated with HGF. **j**, **k**, Bacterial load in gut tissue five days after inoculation of KIE16P (**j**) and *Flip*$^{LysMΔ/Δ}$ (**k**) mice with a 1:1 mix of wild-type CC4 or CC4Δ*inlB* (oral, 2×10^8 CFU (**j**); intravenous, 1×10^4 CFU (**k**)). SI, small intestine. **l**, Schematic representation of InlB-mediated blockade of CD8$^+$ T cell-mediated cell death resulting in neuroinvasion and intestinal persistence. MHC-I, major histocompatibility complex class I; TCR, T cell receptor. *$P < 0.05$, **$P < 0.01$, ***$P < 0.001$, ****$P < 0.0001$; NS, not significant ($P > 0.05$); see the 'Statistical analysis' section for statistical tests. CFU data corresponding to competition indexes are shown in Extended Data Figs. 2, 7, 10.

InlB blocks Fas-mediated cell death

CD8$^+$ T cell cytotoxicity relies on the perforin–granzyme and Fas ligand (FasL)–Fas pathways[24]. InlB-mediated protection against the killing of infected monocytes by CD8$^+$ T cells is fully preserved in perforin-deficient mice (Fig. 3g). In sharp contrast, the inhibitory effect of InlB on the cell death of infected monocytes is fully abrogated in Fas-deficient mice (Fig. 3h), indicating that InlB blocks Fas-mediated killing but has no effect on the perforin pathway. Consistently, monocytes infected with wild-type *Lm*—but not those infected with *LmΔinlB*—are resistant to FasL-induced cell death, whereas surface expression of Fas is not affected by InlB (Fig. 3j, Extended Data Fig. 6f, g). Accordingly, in mice treated with a pharmacological inhibitor of caspase-8 (the downstream effector of Fas[25]), cell death in *LmΔinlB*-infected monocytes is reduced to the levels in wild-type-*Lm*-infected monocytes, and *LmΔinlB* becomes as neuroinvasive as wild-type *Lm* (Fig. 3i, k, Extended Data Fig. 6h, i). The in vivo half-life of monocytes infected with wild-type *Lm* is 50% longer compared to *LmΔinlB*-infected cells, whereas these half-lives are equal and longer in *Rag2*$^{-/-}$ mice, which lack functional lymphocytes including CD8$^+$ T cells (Extended Data Fig. 6j). Moreover, almost 50 times more wild-type-*Lm*-infected monocytes than *LmΔinlB*-infected monocytes adhere to brain blood vessels (Extended Data Fig. 6k, l). In *Rag2*$^{-/-}$ mice, the same number of wild-type-*Lm*- and *LmΔinlB*-infected monocytes circulate in the blood and adhere to the brain vessels (Fig. 3c, Extended Data Figs. 4f, g, 6k, l). Together, these results show that InlB blocks the Fas-mediated killing of infected monocytes by CD8$^+$ T cells, which thereby increases their lifespan and provides them with the necessary time to adhere to brain vessels and transfer intracellular *Lm* to the brain parenchyma.

InlB blocks killing through c-Met–PI3Kα–FLIP

Lm surface-associated InlB mediates the recruitment of its receptor c-Met[26] both in cultured cells[27] and in vivo in *Lm*-infected monocytes, around bacteria both at the cell surface and intracellularly; also recruited are the lysosome-associated membrane glycoprotein LAMP-1 and the adaptor protein GAB1, which is involved in c-Met signalling[28] (Extended Data Fig. 7a–g, Supplementary Videos 4, 5). This suggests that a substantial fraction of InlB-mediated c-Met signalling arises from intravacuolar *Lm*, and, in line with this, an InlB construct that cannot associate to the bacterial surface and therefore cannot recruit c-Met in vacuoles is unable to mediate neuroinvasion (Extended Data Figs. 6a–c, 7b). Consistent with c-Met having a critical role, its competitive inhibition by capmatinib abrogates InlB-mediated neuroinvasion (Fig. 4a, Extended Data Fig. 7h), and InlB-mediated neuroinvasion is abrogated in mice in which *Met* is conditionally deleted in myeloid cells (*LysM*-CreER^{T2} × *Met*$^{flox/+}$ and *LysM*-CreER^{T2} × *Met*$^{flox/flox}$; Fig. 4b, c, Extended Data Fig. 7a, i). Once activated by InlB, c-Met signals through PI3 kinase (PI3K), which leads to the phosphorylation of AKT in infected monocytes[29,30] (Extended Data Fig. 8a, b, Supplementary Video 6). InlB-mediated neuroinvasion is fully blocked by the pan-PI3K inhibitor wortmannin (Extended Data Fig. 8c–d). Specifically, the inhibition of PI3Kα (using BYL-719), but not that of leucocyte-specific PI3Kδ (using IC87114), abrogates InlB-mediated neuroinvasion (Fig. 4d, Extended Data Fig. 8e, f). FLIP, a competitive inhibitor of procaspase-8 that is upregulated by PI3K[24,25], is upregulated in infected monocytes in an InlB dose-dependent manner, which results in a decrease in the activity of caspase-8 (Fig. 4e, f, Extended Data Fig. 8g, h). Pharmacological inhibition of either c-Met or PI3Kα also limits the InlB-mediated upregulation of FLIP and the blocking of caspase-8 activity (Fig. 4e, f). Similarly, FLIP expression is significantly decreased in infected monocytes of *LysM*-CreER^{T2} × *Met*$^{flox/flox}$ mice compared to littermates (Extended Data Fig. 8i), confirming genetically that c-Met is involved in the InlB-mediated upregulation of FLIP in infected monocytes. The InlB-mediated resistance of infected monocytes to cell death is lost in mice that lack *Flip* (also known as *Cflar*) (*Rosa*-CreER^{T2} × *Flip*$^{flox/flox}$; Fig. 4g, Extended Data Fig. 8j) and the involvement of InlB in neuroinvasion is fully abrogated in mice that are conditionally deleted for *Flip* in myeloid cells (*LysM*-CreER^{T2} × *Flip*$^{flox/+}$ and *LysM*-CreER^{T2} × *Flip*$^{flox/flox}$; Fig. 4h, Extended Data Fig. 8k, l), showing that the inhibition of cell death that is mediated by InlB-dependent upregulation of FLIP is responsible for the increased neuroinvasion of *Lm* in vivo. Finally, in vivo exogenous activation of c-Met by its ligand hepatocyte growth factor (HGF) leads to the upregulation of FLIP expression, protects infected monocytes from cell death and renders *Lm*Δ*inlB* as neuroinvasive as wild-type *Lm* (Fig 4i, Extended Data Fig. 8m–o). InlB-mediated blockade of the Fas cell death pathway in infected monocytes therefore results from the InlB-, c-Met- and PI3Kα-dependent cell-autonomous upregulation of the caspase-8 inhibitor FLIP (Extended Data Fig. 9a), which extends the half-life of infected monocytes and therefore promotes neuroinvasion.

InlB promotes intestinal persistence of *Lm*

InlB is part of the *Lm* core genome and is under purifying selection[17,31], which suggests that it confers a selective advantage to *Lm*. As *Lm* is shed back from infected tissues into the intestinal lumen[32], increased virulence of *Lm* may translate into increased faecal shedding and favour transmission. We therefore tested whether InlB is involved in the persistence of *Lm* in the intestines and its release in the faeces after oral and intravenous inoculation. Indeed, the levels of infection of intestinal tissues and release in the intestinal lumen and faeces were significantly higher for wild-type *Lm* than for *Lm*Δ*inlB* (Fig. 4j, k, Extended Data Fig. 9b–d). At 5 dpi, mice that were infected with wild-type *Lm* had significantly more infected myeloid cells in the lamina propria (CD11b$^+$CX3CR1$^+$; more than 80% of infected cells of the intestine) than did mice infected with *Lm*Δ*inlB* (Extended Data Fig. 9e–g, Supplementary Videos 7, 8). As with neuroinvasion, these differences are fully dependent on CD8$^+$ T cells, on FLIP expressed in myeloid cells and on InlB-dependent blocking of caspase-8-mediated cell death (Fig. 4k, Extended Data Fig. 10). These observations show that InlB specific interference with adaptive immunity promotes *Lm* within-host persistence and faecal shedding (Fig 4l).

Discussion

We have shown here that *Lm* renders infected host cells resistant to CD8$^+$ T cell-mediated killing. Selective blockade of the Fas–FasL death pathway in infected monocytes allows these cells to survive longer in the blood and to transfer *Lm* more abundantly to the brain. Notably, this unanticipated mechanism, which creates an intracellular protected niche for *Lm*, is also involved in its persistence in the intestinal tissue and its release in the faeces and, ultimately, in the environment. This mechanism is mediated by the *Lm* surface protein InlB, which was previously described as being involved in the internalization of *Lm* into non-phagocytic cells. We reveal here the key role of InlB as an immunomodulatory protein. InlB promotes the survival of monocytes and neuroinvasion through the upregulation—through a c-Met- and PI3Kα-dependent pathway—of FLIP, the competitive inhibitor of procaspase-8; this competitively inhibits the cleavage of caspase-8 and thereby blocks FasL–Fas-mediated cell death.

Our study highlights the important role of cellular immunity against the neuroinvasion of intracellular pathogens from a microbial perspective. Whereas extracellular pathogens rely on binding to specific host cell receptors[33] or breaching of host barriers[34] to invade the CNS, the facultative intracellular pathogen *Lm* takes advantage of its ability to persist within host cells through InlB-mediated immunoresistance to favour its crossing of the blood–brain barrier via ActA. These results show that the capacity of microorganisms to survive within cells is a key pathogenic determinant that favours within-host dissemination and ultimately neuroinvasion. Other neuroinvasive intracellular pathogens such as *Mycobacterium tuberculosis* and *Toxoplasma gondii* also stimulate PI3K[35,36] and survive in myeloid cells[35,36], suggesting that they may also protect infected cells from cell death, thus promoting their survival and increasing their within-host persistence and neuroinvasiveness.

Intracellular pathogens establish a successful infection by interfering with innate immune responses, and some also persist in the host by interfering with the adaptive immune system in a broad and non-selective manner; for example, HIV, Epstein–Barr virus and measles virus[37,38]. *Lm* has been instrumental for the discovery of cellular immunity[39] and is indeed a prototypic inducer of a protective CD8$^+$ T cell response[40,41]. Yet we show here that InlB selectively impairs the action of the most efficient and specific anti-*Lm* immune effector, T cell-mediated cytotoxicity, creating a protected cellular niche that favours the dissemination of *Lm* and its persistence within the host. This is reminiscent of the mechanism by which tumour cells—in which signalling downstream of growth factor receptors is frequently constitutively activated[42,43]—also evade immune responses by surviving immune killing. A detailed understanding of how microorganisms have selected mechanisms that interfere with the immune system may help in the rational design of anti-infective and anti-tumour therapies. Similarly, the immunomodulatory mechanism of InlB—specific and restricted to infected cells—may also help in the development of immunosuppressive strategies that are aimed at specifically protecting cells of interest from immune killing, as opposed to classic immunosuppressive drugs that inhibit immune functions in an indiscriminate manner and can result in infectious and neoplastic complications.

Lm is an opportunistic pathogen that only rarely induces a clinically apparent infection after oral ingestion[44], and there is no inter-human horizontal transmission of listeriosis. However, the so-called 'virulence

factors' of *Lm* are under purifying selection[17,31,45], which suggests that they contribute to the fitness of *Lm*. By interfering with the anti-*Lm* cellular effectors of the host, InlB enhances *Lm* intestinal colonization and faecal shedding, which increases the chances of neuroinvasive *Lm* being transmitted back to the environment and colonizing new hosts. This indicates that the anthropocentric view on microbial pathogenesis, in which phenotypic output is centred on disease, does not necessarily reflect the actual context in which microbial evolution and fitness gain take place.

Online content

Any methods, additional references, Nature Research reporting summaries, source data, extended data, supplementary information, acknowledgements, peer review information; details of author contributions and competing interests; and statements of data and code availability are available at https://doi.org/10.1038/s41586-022-04505-7.

1. Schuchat, A. et al. Bacterial meningitis in the United States in 1995. *N. Engl. J. Med.* **337**, 970–976 (1997).
2. van de Beek, D. et al. Clinical features and prognostic factors in adults with bacterial meningitis. *N. Engl. J. Med.* **351**, 1849–1859 (2004).
3. Charlier, C. et al. Clinical features and prognostic factors of listeriosis: the MONALISA national prospective cohort study. *Lancet Infect. Dis.* **17**, 510–519 (2017).
4. Mailles, A. & Stahl, J. Infectious encephalitis in France in 2007: a national prospective study. *Clin. Infect. Dis.* **49**, 1838–1847 (2009).
5. Skogberg, K. et al. Clinical presentation and outcome of listeriosis in patients with and without immunosuppressive therapy. *Clin. Infect. Dis.* **14**, 815–821 (1992).
6. Maury, M. M. et al. Uncovering *Listeria monocytogenes* hypervirulence by harnessing its biodiversity. *Nat. Genet.* **48**, 308–313 (2016).
7. Disson, O. et al. Conjugated action of two species-specific invasion proteins for fetoplacental listeriosis. *Nature* **455**, 1114–1118 (2008).
8. Drevets, D. A., Jelinek, T. A. & Freitag, N. E. *Listeria monocytogenes*-infected phagocytes can initiate central nervous system infection in mice. *Infect. Immun.* **69**, 1344–1350 (2001).
9. Join-Lambert, O. F. et al. *Listeria monocytogenes*-infected bone marrow myeloid cells promote bacterial invasion of the central nervous system. *Cell. Microbiol.* **7**, 167–180 (2005).
10. Cantinelli, T. et al. "Epidemic clones" of *Listeria monocytogenes* are widespread and ancient clonal groups. *J. Clin. Microbiol.* **51**, 3770–3779 (2013).
11. Bécavin, C. et al. Comparison of widely used *Listeria monocytogenes* strains EGD, 10403S, and EGD-e highlights genomic variations underlying differences in pathogenicity. *mBio* **5**, e00969-14 (2014).
12. Pizarro-Cerdá, J., Lecuit, M. & Cossart, P. in *Molecular Cellular Microbiology* Vol. 31 (eds Sansonetti, P. & Zychlinsky, A.) 161–177 (Academic Press, 2002).
13. Boring, L. et al. Impaired monocyte migration and reduced type 1 (Th1) cytokine responses in C-C chemokine receptor 2 knockout mice. *J. Clin. Invest.* **100**, 2552–2561 (1997).
14. Kocks, C. et al. *L. monocytogenes*-induced actin assembly requires the *actA* gene product, a surface protein. *Cell* **68**, 521–531 (1992).
15. Tilney, L. G. & Portnoy, D. A. Actin filaments and the growth, movement, and spread of the intracellular bacterial parasite, *Listeria monocytogenes*. *J. Cell Biol.* **109**, 1597–1608 (1989).
16. Lecuit, M. et al. A transgenic model for listeriosis: role of internalin in crossing the intestinal barrier. *Science* **292**, 1722–1725 (2001).
17. Moura, A. et al. Whole genome-based population biology and epidemiological surveillance of *Listeria monocytogenes*. *Nat. Microbiol.* **2**, 16185 (2016).
18. Gaillard, J. L., Jaubert, F. & Berche, P. The *inlAB* locus mediates the entry of *Listeria monocytogenes* into hepatocytes in vivo. *J. Exp. Med.* **183**, 359–369 (1996).
19. Braun, L. et al. InlB: an invasion protein of *Listeria monocytogenes* with a novel type of surface association. *Mol. Microbiol.* **25**, 285–294 (1997).
20. Dramsi, S. et al. Entry of *Listeria monocytogenes* into hepatocytes requires expression of InlB, a surface protein of the internalin multigene family. *Mol. Microbiol.* **16**, 251–261 (1995).
21. Lane, F. C. & Unanue, E. R. Requirement of thymus (T) lymphocytes for resistance to listeriosis. *J. Exp. Med.* **135**, 1104–1112 (1972).
22. Schlüter, D. et al. Systemic immunization induces protective $CD4^+$ and $CD8^+$ T cell-mediated immune responses in murine *Listeria monocytogenes* meningoencephalitis. *Eur. J. Immunol.* **25**, 2384–2391 (1995).
23. Khanna, K. M., McNamara, J. T. & Lefrançois, L. In situ imaging of the endogenous CD8 T cell response to infection. *Science* **318**, 116–120 (2007).
24. Doherty, P. Cell-mediated cytotoxicity. *Cell* **75**, 607–612 (1993).
25. Muzio, M. et al. FLICE, a novel FADD-homologous ICE/CED-3-like protease, is recruited to the CD95 (Fas/APO-1) death-inducing signaling complex. *Cell* **85**, 817–827 (1996).
26. Shen, Y., Naujokas, M., Park, M. & Ireton, K. InlB-dependent internalization of *Listeria* is mediated by the Met receptor tyrosine kinase. *Cell* **103**, 501–510 (2000).
27. Bierne, H. et al. A role for cofilin and LIM kinase in *Listeria*-induced phagocytosis. *J. Cell Biol.* **155**, 101 (2001).
28. Weidner, K. M. et al. Interaction between Gab1 and the c-Met receptor tyrosine kinase is responsible for epithelial morphogenesis. *Nature* **384**, 173–176 (1996).
29. Bowers, D. C. et al. Scatter factor/hepatocyte growth factor protects against cytotoxic death in human glioblastoma via phosphatidylinositol 3-kinase- and AKT-dependent pathways. *Cancer Res.* **60**, 4277–4283 (2000).
30. Xiao, G.-H. et al. Anti-apoptotic signaling by hepatocyte growth factor/Met via the phosphatidylinositol 3-kinase/Akt and mitogen-activated protein kinase pathways. *Proc. Natl Acad. Sci. USA* **98**, 247–252 (2001).
31. Tsai, Y. H. L., Orsi, R. H., Nightingale, K. K. & Wiedmann, M. *Listeria monocytogenes* internalins are highly diverse and evolved by recombination and positive selection. *Infect. Genet. Evol.* **6**, 378–389 (2006).
32. Louie, A., Zhang, T., Becattini, S., Waldor, M. K. & Portnoy, D. A. A multiorgan trafficking circuit provides purifying selection of *Listeria monocytogenes* virulence genes. *mBio* **10**, e02948-19 (2019).
33. Coureuil, M., Lécuyer, H., Bourdoulous, S. & Nassif, X. A journey into the brain: insight into how bacterial pathogens cross blood–brain barriers. *Nat. Rev. Microbiol.* **15**, 149–159 (2017).
34. Devraj, G. et al. HIF-1α is involved in blood–brain barrier dysfunction and paracellular migration of bacteria in pneumococcal meningitis. *Acta Neuropathol.* **140**, 183–208 (2020).
35. Liu, Y., Li, J. Y., Chen, S. T., Huang, H. R. & Cai, H. The rLrp of *Mycobacterium tuberculosis* inhibits proinflammatory cytokine production and downregulates APC function in mouse macrophages via a TLR2-mediated PI3K/Akt pathway activation-dependent mechanism. *Cell. Mol. Immunol.* **13**, 729–746 (2016).
36. Quan, J. H. et al. Intracellular networks of the PI3K/AKT and MAPK pathways for regulating *Toxoplasma gondii*-induced IL-23 and IL-12 production in human THP-1 cells. *PLoS One* **10**, e0141550 (2015).
37. Klenerman, P. & Hill, A. T cells and viral persistence: lessons from diverse infections. *Nat. Immunol.* **6**, 873–879 (2005).
38. Protzer, U., Maini, M. K. & Knolle, P. A. Living in the liver: hepatic infections. *Nat. Rev. Immunol.* **12**, 201–213 (2012).
39. Mackaness, G. B. Cellular resistance to infection. *J. Exp. Med.* **116**, 381–406 (1962).
40. Pamer, E. G. Immune responses to *Listeria monocytogenes*. *Nat. Rev. Immunol.* **4**, 812–823 (2004).
41. Shen, H. et al. Recombinant *Listeria monocytogenes* as a live vaccine vehicle for the induction of protective anti-viral cell-mediated immunity. *Proc. Natl Acad. Sci. USA* **92**, 3987–3991 (2006).
42. Spranger, S., Bao, R. & Gajewski, T. F. Melanoma-intrinsic β-catenin signalling prevents anti-tumour immunity. *Nature* **523**, 231–235 (2015).
43. Tauriello, D. V. F. et al. TGFβ drives immune evasion in genetically reconstituted colon cancer metastasis. *Nature* **554**, 538–543 (2018).
44. Ricci, A. et al. *Listeria monocytogenes* contamination of ready-to-eat foods and the risk for human health in the EU. *EFSA J.* **16**, 5134 (2018).
45. Maury, M. M. et al. Spontaneous loss of virulence in natural populations of *Listeria monocytogenes*. *Infect. Immun.* **85**, e00541-17 (2017).

Methods

Mice

Animal experiments were performed according to the Institut Pasteur guidelines for laboratory animal husbandry and in compliance with the 2010/63 EU European regulations. All procedures were approved by the Animal Ethics Committee of the Institut Pasteur, authorized by the French Ministry of Research and registered under no. 11995-201703115103592 and no. 14644-2018041116183944.

C57BL/6JRj and BALB/c mice were purchased from Janvier Labs and bred at the Institut Pasteur. KIE16P mice expressing humanized E16P E-cadherin[7], iFABP-hEcad mice[16], *Rag2*$^{-/-}$ mice[46], CD3ε$^{-/-}$ mice[47], muMt$^{-/-}$ mice[48], *Ccr2*$^{-/-}$ mice[13], $CX_3CR1^{+/GFP}$ mice[49], *Rosa26*-CreER^{T2} mice[50] and *Rosa26*-iDTR[51] were bred at the Institut Pasteur. *Fas*$^{lpr\text{-}cg}$ mice, carrying a spontaneous mutation at the *Fas* locus[52], and *Prf1* KO mice, deleted for the perforin gene[53], were obtained from F. Rieux-Laucat and F. Sepulveda, respectively. *Cflar*$^{flox/flox}$ (*Flip*$^{flox/flox}$) mice[54] were obtained from R. M. Pope, *Met*$^{flox/flox}$ mice[55] from A. Eychene and *LysM*-CreER^{T2} mice[56] from F. Greten.

Mice were housed in groups of up to seven mice, in a BSL-3 animal facility, on poplar chips (SAFE, D0736P00Z) and were fed with irradiated food at 25 kGy (SAFE, 150SP-25). The facility has central air conditioning equipment that maintains a constant temperature of 22 ± 2 °C. Air is renewed at least 20 times per hour in animal rooms. Light is provided with a 14:10-h light:dark cycle (06:30 to 20:30). Mice were kept in polypropylene or polycarbonate cages that comply with European regulations in terms of floor surface per animal. All cages were covered with stainless steel grids and non-woven filter caps.

All experiments were performed on mice between 7 and 12 weeks of age, which were randomly assigned to each different condition without blinding. Unless stated otherwise in the figure legends, 'mice' refers to KIE16P mice. Only female mice were used throughout the study, except for experiments involving *Flip*$^{flox/flox}$ × *LysM*-CreER^{T2} and *Met*$^{flox/flox}$ × *LysM*-CreER^{T2} mice, for which both male and female mice were included.

No sample size calculations were performed. The sample size (n) of each experiment is provided in Supplementary Table 7 for the main figures and also on each panel as each dot corresponds to one mouse (sample). Sample sizes were chosen to support meaningful conclusions with the statistical tests used. We used around 8–14 mice per group, a number sufficient to reach statistical significance using non-parametric statistical tests with the effect size we expected to observe, on the basis of our previous observations.

Bacterial strains

All of the bacterial strains used in this study are presented in Supplementary Table 2. To obtain growth curves, bacteria grown overnight in brain heart infusion (BHI) (with chloramphenicol when needed), at 37 °C and 200 rpm, were diluted 1:100 in BHI (with chloramphenicol when needed), incubated at 37 °C and 200 rpm, and the optical density at 600 nm ($OD_{600\,nm}$) was measured every hour for 9 h. Growth curves were fitted using the Gompertz model to compare parameters between each strain.

Mutagenesis and plasmids

The oligonucleotide primers and plasmids used in this study are listed in Supplementary Tables 3 and 4, respectively. Deletion mutants were constructed as described previously[57]. The flanking regions of the target genes were PCR-amplified. After purification, the fragments were stitched together by sequence overlap extension, then cloned into the pMAD shuttle vector[58]. The vector was then electroporated into electrocompetent *Lm* cells. After plasmid integration and excision by sequence homology, gene deletion was verified by sequencing the PCR product of the target region. For *Lm*Δ*inlA* mutants, to avoid alteration of InlB expression in the operon, the *inlA* gene with flanking regions was PCR-amplified and cloned into the pLR16-pheS plasmid[59] (a gift from A. Herskovits) and a point mutation was introduced by PCR in the *inlA* gene, resulting in a premature stop codon. The plasmid was then purified and electroporated into electrocompetent *Lm*Δ*inlA* bacteria. After plasmid integration and excision by sequence homology, allele replacement was verified by sequencing the PCR product of the target region.

The pAD backbone[60], integrated as a single copy at the tRNAArg-attBB site into the *Listeria* genome, was used to allow the expression of tdTomato and GFP. First, an EcoRV restriction site was added in pAD between the 5′ untranslated region of *hly* and the ATG start codon, generating the plasmid pCMC12. tdTomato and GFP sequences were codon-optimized for expression in *Lm* using Optimizer (http://genomes.urv.es/OPTIMIZER/), synthesized by Eurofins with EcoRV and SalI flanking restriction sites and inserted in pCMC12 between EcoRV and SalI sites. *inlB* sequences were amplified from EGDe (MBHL0005), CC4 (MBHL0257) and *Listeria innocua* BUG1642 (MBHL0052, expressing a construct in which the InlB anchoring region is replaced by the anchoring domain of the *Staphylococcus aureus* protein A[19]) genomic DNAs and were inserted in pCMC12 between EcoRV and SalI sites. The promoter in pCMC12 is pHyper, a strong constitutive promoter that allows an in vivo expression level of InlB in complemented strains that is equivalent to that of hypervirulent strains. The β-lactamase construct has been described previously[61]. All constructs were electroporated into electrocompetent *Lm* cells. Integration was verified by PCR.

Infections and bacterial enumeration

Bacterial inocula were prepared by centrifugation of a bacterial culture grown in BHI, at 37 °C and shaken at 200 rpm, until an $OD_{600\,nm}$ of 0.8 (8×10^8 viable bacteria per ml) was reached; then washed in phosphate-buffered saline (PBS) and resuspended in PBS at the appropriate dilution. For oral inoculation, 0.2 ml of bacteria (2×10^8 CFU, unless specified otherwise) was mixed with 0.3 ml of PBS containing 50 mg ml^{-1} $CaCO_3$ (Sigma) and injected intragastrically through a feeding needle (ECIMED) to isoflurane-anaesthetized mice. For intravenous infection, 0.1 ml of bacteria (10^4 CFUs, unless specified otherwise) were injected in the tail vein using a 25G needle.

For intracerebral infections, mice were anaesthetized in 3% isoflurane, then received 10 µl of bacterial suspension by intracranial injection using a 26G needle inserted approximately 2 mm anterior to the bregma, 1 mm laterally and 1.5 mm ventrally; this corresponds to the frontal motor cortex as it is the most easily accessible part of the brain for reproducible intracranial inoculation, and as it avoids major blood vessels.

For immunization experiments, mice were first infected with wild-type or Δ*inlB* strains by oral gavage with 5×10^7 CFU. After 30 days, mice were then infected intragastrically for the second challenge with 2×10^9 wild-type bacteria for 3 days.

At the indicated times, mice were euthanized, either through CO_2 exposure or ketamine or xylazine overdose, and transcardial perfusion was performed when flushing of the vasculature was necessary (Extended Data Fig. 1l). Organs were aseptically collected. The intestine, colon and caecum were incubated with gentamicin (100 µg ml^{-1}) for 2 h to eliminate extra-tissular bacteria. All organs were homogenized in PBS with a tissue homogenizer (UltraTurrax T-25 basic, IKA works). Serial dilutions of the homogenate were plated onto BHI agar (or ALOA for faeces and intestinal content) and the CFU was enumerated. CFU is expressed per ml for blood and per whole organ otherwise. CFU in the brain comprises both the CFU in the parenchyma and the CFU in the meninges.

Competition index experiments were performed as described previously[62]. In brief, a 1:1 ratio of wild-type bacteria, expressing tdTomato, and mutant bacteria, expressing GFP, was injected into mice, confirmed by CFU enumeration of the inoculum onto BHI agar. Wild-type and mutant bacteria CFU were distinguished by colony colour on BHI agar.

Competition index is calculated as the ratio of wild-type versus mutant CFU in each organ. Mice with a bacterial load lower than 10 CFU were not included for the calculation of competition indexes, as it may induce a bias, but are presented in the corresponding CFU graphs to show the global level of neuroinvasion. Unless stated otherwise, competition indexes were performed five days after inoculation—a time point late enough to have consistent CNS invasion and induction of adaptive immune responses but before humane end-points were reached. Whenever the mouse strains were permissive to *Lm* oral infection, intragastric inoculation was used for competition index assays.

Drug treatments of mice

All drugs used in this study and their mode of delivery are presented in Supplementary Table 5.

Gentamicin was administered intraperitoneally every day from 1 dpi to assess the contribution of intracellular bacteria to brain infection, except in Extended Data Fig. 1b, for which it was intravenously injected immediately after intravenous infection with extracellular *Lm*, to demonstrate the bactericidal effect of gentamicin on extracellular bacteria.

For in vivo HGF administration, owing to the extremely short half-life of HGF, recombinant mouse HGF (Biolegend) was administered using a micro-osmotic pump (Model 1003D, Alzet), inserted subcutaneously under isoflurane anaesthesia as described previously[63]. The pumps were loaded with 100 µl of mouse HGF in PBS (150 µg ml^{-1}) or PBS alone with a delivery rate of approximately 1 µl per hour over a 3-day period.

RNA isolation and quantitative PCR with reverse transcription

For in vitro analysis, bacteria were grown in BHI at 37 °C and 200 rpm until $OD_{600\ nm}$ = 0.8. They were then centrifuged, lysed in resuspension buffer (10% glucose, 12.5 mM Tris, 10 mM EDTA in nuclease-free water), transferred into a Precellys tube (Ozyme) containing 0.1-mm ceramic beads (Ozyme) and acid phenol (Sigma) and homogenized using a Precellys 24 apparatus (Ozyme). The aqueous phase was transferred into a new tube containing TRIzol (Invitrogen) and chloroform (Sigma), shaken and centrifuged at maximum speed at 4 °C for 15 min. The aqueous phase was transferred into a new tube containing chloroform, shaken and centrifuged at maximum speed at 4 °C for 15 min. The aqueous phase was transferred into a new tube containing 1 volume of isopropanol (Sigma) and 0.1 volumes of 3M sodium acetate (Sigma), and incubated for at least 20 min at −20 °C.

For in vivo analysis, spleens were collected aseptically, and single-cell suspensions were obtained by homogenizing through a 40-µm cell strainer. Cells were lysed in TRIzol and chloroform, shaken and centrifuged at maximum speed at 4 °C for 15 min. The aqueous phase was transferred into a new tube containing 1 volume of isopropanol, and incubated for at least 20 min at −20 °C.

For both in vitro and in vivo samples, RNAs were pelleted at maximum speed at 4 °C for at least 20 min and washed three times in 80% ethanol (Sigma), air-dried and dissolved in RNase-free water. Total RNA was reverse-transcribed using hexameric random primers (Invitrogen) and M-MLV reverse transcriptase (Invitrogen) following the manufacturer's instructions. Quantification of gene expression was performed using Power SYBR Green PCR Master Mix, a Step-One Real-Time PCR apparatus (both from Applied Biosystems) and the primers listed in Supplementary Table 3. Expression of *inlA* and *inlB* was normalized to that of *gyrB* and compared to EGDe using the $\Delta\Delta C_T$ method.

Flow cytometry

Mice were euthanized at the indicated times post-infection. Functional characterization of CD8$^+$ T cells and infected monocytes were performed after intravenous inoculation, unless stated otherwise, which allows for less intra-mouse variation and thus reduces the number of mice needed for experiments. Counting and characterization of infected cells in the blood and spleen were performed at 4 dpi (both orally and intravenously), when bacteraemia is the highest. For orally infected mice, as the bacteraemia was very low even at 4 dpi, the blood of three mice was pooled and analysed as one sample. Counting and characterization of infected cells in the intestine was performed after intravenous inoculation, to avoid early infection events linked to the inoculum passage of the intestinal barrier after oral inoculation, at 5 dpi, a time when the bacterial load is sufficient to detect late infection events. For cell-death-related experiments and characterization of infected inflammatory monocytes, we collected the spleen at 3 dpi, the earliest time point at which the effect of InlB is consistently observed, but also when cell death is moderate in the spleen, so that we could collect a sufficient number of viable cells. Spleens, livers, mesenteric lymph nodes (MLNs) and blood (by cardiac puncture in heparin-coated syringe) were collected aseptically. Single-cell suspensions were obtained from spleen and MLNs by homogenizing through a 40-µm cell strainer. Single-cell suspensions were obtained from liver using the Multi Tissue Dissociation Kit 1 (Miltenyi Biotec) and MACS apparatus (Miltenyi Biotec) following the manufacturer's instructions and successive filtration through 70- and 40-µm cell strainers. After red blood cell lysis using 1× RBC lysis buffer (eBiosciences), the cells were washed in cell staining buffer (CSB) (BioLegend) before further processing.

Small intestines were collected without conjunctive tissue, opened longitudinally, washed in ice-cold PBS, cut into 1–1.5-cm pieces and washed again in ice-cold PBS. Epithelial cells were first isolated after incubation of intestinal pieces in HBSS (Invitrogen) with 5% fetal calf serum (FCS), 10 mM HEPES (Sigma) and 5 mM EDTA for 3 times 20 min at 37 °C with 200 rpm shaking. After washing in ice-cold DMEM (Invitrogen), leukocytes of the lamina propria were isolated after incubation in DMEM with DNase I (Roche) and Liberase TL (Roche) for 45 min at 37 °C with 200 rpm shaking. Single-cell suspensions of epithelial cells and leukocytes from the lamina propria were filtered successively through 100-, 70- and 40-µm cell strainers, washed in ice-cold DMEM then in CSB, and processed further separately.

If required, cells were labelled using the LiveBLAzer FRET-B/G Loading Kit with CCF2-AM (Invitrogen), a fluorescent substrate of β-lactamase that can cross the plasma membrane. The presence of β-lactamase-expressing bacteria in cells induces a shift in the fluorescence emission of the CCF2-AM substrate from 518 nM (green) to 447 nM (blue) upon excitation with the 405 nM laser and thus allows for identification of infected cells. Cells were loaded with the CCF2-AM substrate following the manufacturer's instructions for 2 h 30 min at room temperature in CSB containing 1 mM probenecid (Sigma). After washing, cells were blocked using CD16/32 (BioLegend) for 5 min at room temperature, washed in CSB, stained with the appropriate antibodies (listed in Supplementary Table 6) for 45 min at 4 °C and washed in CSB. If no intracellular staining was required, cells were suspended in CSB containing CountCAL beads (Sony) for absolute counting of cells. For intracellular staining, cells were fixed for 20 min at room temperature in IC fixation buffer (eBiosciences), washed three times in 1× permeabilization buffer (eBiosciences), incubated with primary antibodies for 1 h at room temperature, washed and incubated with secondary antibodies for 45 min at room temperature. After washing, cells were suspended in CSB containing CountCAL beads for absolute counting of cells. Cells were acquired on a Fortessa X-20 SORP apparatus (BD biosciences) and analysed using FlowJo software (TreeStar). B cells were defined as CD45$^+$CD19$^+$CD3$^-$; CD8$^+$ T cells as CD45$^+$CD3$^+$CD8$^+$CD19$^-$; LLO-specific CD8$^+$ T cells as CD45$^+$CD3$^+$CD8$^+$LLO-pentamer$^+$CD19$^-$; CD4$^+$ T cells as CD45$^+$CD3$^+$CD4$^+$CD19−; granulocytes as CD45$^+$Ly6G$^+$CD3$^-$CD19$^-$; patrolling monocytes in blood as CD45$^+$CD11b$^+$CD11c$^+$CD3$^-$CD19$^-$Ly6G$^-$Ly6C$^-$; inflammatory monocytes as CD45$^+$CD11b$^+$Ly6C^{high}CD3$^-$CD19$^-$Ly6G$^-$CD11c$^-$; macrophages in spleen as CD45$^+$CD11b$^+$CD11c$^+$CD3$^-$CD19$^-$Ly6G$^-$Ly6C$^-$; dendritic cells in spleen as CD45$^+$CD11c$^+$CD3$^-$CD19$^-$Ly6G$^-$Ly6C$^-$; macrophages in lamina propria as CD45$^+$CD11b$^+$CX3CR1$^+$CD3$^-$CD19$^-$Ly6G$^-$CD11c$^-$; dendritic cells in lamina propria as CD45$^+$CD11c$^+$CD103$^+$CD3

$^{-}$CD19^{-}Ly6G^{-}Ly6C^{-}; epithelial cells in the intestine as Ep-Cam^{+}CD45^{-}; dying cells as Zombie NIR^{+}; infected cells as CCF2-blue and non-infected cells as CFF2-green. The number of cells is expressed per ml of blood, per spleen or per small intestine.

CTL assays

Infected mice were euthanized at 3 dpi, a time point at which activated CD8^{+} T cells are already present but before cell death is induced in infected monocytes. Spleens were collected aseptically and cells prepared as described above for flow cytometry, resuspended in CSB and sorted on a FACSAria III apparatus (BD Biosciences) into FCS-containing tubes. Activated CD8^{+} T cells were defined as CD45^{+}CD3^{+}CD8^{+}CD69^{+}CD19^{-}; infected inflammatory monocytes as CD45^{+}CD11b^{+}Ly6C^{high}CD3^{-}CD19^{-}Ly6G^{-}CD11c^{-}CCF2-blue; and non-infected inflammatory monocytes as CD45^{+}CD11b^{+}Ly-6C^{high}CD3^{-}CD19^{-}Ly6G^{-}CD11c^{-}CCF2-green. For mock-treated mice, CD8^{+} T cells and inflammatory monocytes were sorted. After sorting, cells were washed and resuspended in RPMI medium (Invitrogen) containing 10% FCS. Activated CD8^{+} T cells and monocytes (infected and non-infected), isolated from independent mice, were co-incubated at the indicated ratio for 80 min at 37 °C, washed and fixed with IC fixation buffer overnight at 4 °C. After three washes in 1× permeabilization buffer, cells were stained with anti-cleaved caspase-3 antibody for 1 h at room temperature, washed and stained with secondary antibody for 45 min at room temperature. After washing, cells were acquired on an X-20 Fortessa SORP apparatus and the percentage of monocytes positive for cleaved caspase-3 signal was analysed using FlowJo software.

Half-lives of infected monocytes

Mice (B6 wild type or *Rag2*$^{-/-}$) were infected intravenously with 10^4 *Lm* CFUs. At day 2 after inoculation, single-cells suspension were obtained from spleens of non-infected B6 wild-type mice as described in the flow cytometry section. Cells were then labelled with Vybrant DiD solution (Invitrogen) for 20 min at 37 °C, according to the manufacturer's instructions. After three washes in DMEM-F12 medium, cells were resuspended in PBS and immediately transferred into infected mice intravenously, where they could get infected. Mice were euthanized at indicated time points, starting from 12 h post-transfer (arbitrarily defined as time 0) to allow time for transferred monocytes to be infected in vivo in sufficient numbers to be readily detected before assessing their decay. Spleen and blood samples were collected aseptically. Single-cell suspensions were then prepared and loaded with the CCF2-AM substrate and stained as described above. After washing, cells were acquired on an X-20 Fortessa SORP apparatus and the percentage of infected monocytes positive for Vybrant DiD signal was analysed using FlowJo software.

Estimation of the half-lives of infected monocytes from exponential fits

The proportion of infected transferred monocytes (relative to their number at time point 0) in the spleen and blood of recipient mice across time were fitted by a one-phase decay exponential function ($y = K \times \exp(-t/\tau)$). Half-lives were determined as $t_{1/2} = \ln(2)/\tau$, using the τ values from the best-fit parameters for each condition. Values of half-lives were then compared using the extra-sum of squares *F*-test, and the corresponding *P* values reported in the figure.

FasL treatment

Infected mice were euthanized at 3 dpi and spleens were collected aseptically. Cells were prepared and sorted in the same conditions as for CTL assays. Infected and non-infected inflammatory monocytes were sorted into FCS-containing tubes. After sorting, cells were washed and resuspended in RPMI medium containing 10% FCS. Cells were then treated with either HA antibody as control (Cell Signaling) or with HA antibody plus recombinant mouse FasL/TNFSF6 (R&D systems) for 80 min at 37 °C. After washing, cells were fixed overnight in IC fixation buffer. After three washes in 1× permeabilization buffer, cells were stained with anti-cleaved caspase-3 antibody for 1 h at room temperature, washed and stained with secondary antibody for 45 min at room temperature. After washing, cells were acquired on an X-20 Fortessa SORP apparatus and the percentage of monocytes positive for cleaved caspase-3 signal was analysed using FlowJo software.

Caspase-8 activity assay

Mice were inoculated intravenously, treated with either BYL-719 or capmatinib and euthanized at 3 dpi. Single-cell suspensions were prepared from spleen as described in the flow cytometry section. After CCF2-AM loading, blocking with CD16/32 and staining with the appropriate antibodies, cells were incubated for 30 min at 37 °C with Red-IETD-FMK from CaspGLOW Red Active Caspase-8 Staining Kit (Clinisciences), washed and suspended in wash buffer containing CountCAL beads for absolute counting of cells. Cells were immediately acquired on a Fortessa X-20 SORP apparatus and analysed using FlowJo software.

Transfer of infected monocytes into recipient mice

Infected KIE16P mice were euthanized at 3 dpi and spleens were collected aseptically. Cells were prepared as described above and sorted in the same conditions as for CTL assays. Infected monocytes from six mice were sorted into FCS-containing tubes, pooled, washed and injected into a naive mouse treated with gentamicin, corresponding to an inoculum of 10^4 live CFUs. Two days after injection, the mouse was euthanized, the organs were collected aseptically and the bacteria were enumerated as described above.

LysM-CreER$^{T2+/-}$ × *Rosa26*-iDTR$^{+/-}$ and their littermates were infected intravenously with CC4 *Lm*, treated with tamoxifen to allow for Cre expression and euthanized 4 days after infection, and the spleens were collected aseptically. Cells were prepared as described above and sorted in the same conditions as for CTL assays. Infected monocytes from three mice were sorted into FCS-containing tubes, pooled (corresponding to an inoculum of 2×10^4 live CFUs), washed and injected into a naive recipient mouse (same genotype as donor mice) treated with both diphtheria toxin and gentamicin, to kill Cre-expressing monocytes and extracellular bacteria. At 4 dpi, mice were euthanized, the organs were collected aseptically and the bacteria were enumerated as described above.

Bacterial enumeration in infected monocytes

Infected mice were euthanized at 4 dpi, when the bacteraemia is the highest, and spleens and blood were collected aseptically. Cells were prepared as described above and sorted in the same conditions as for CTL assays. Monocytes were collected into FCS-containing tubes, washed and resuspended into 0.1% Triton, serially diluted in PBS and plated on BHI agar.

Immunofluorescence labelling and fluorescence microscopy

Brain hemispheres were fixed in 4% paraformaldehyde in PBS overnight at 4 °C then washed in PBS, embedded in 4% agarose and sectioned into 40-µm-thick slices using a vibrating microtome (Thermo Fisher Scientific, HM 650V).

Slices were washed in PBS, then incubated for 2 h in blocking permeabilization solution (10% goat serum, 4% FCS and 0.4% Triton X-100 in PBS). Tissues were then labelled with the appropriate primary antibodies (listed in Supplementary Table 6) overnight at 4 °C in mild blocking conditions (4% goat serum, 4% FCS and 0.4% Triton X-100 in PBS), washed in PBS, and then incubated with secondary antibodies (listed in Supplementary Table 6), Hoechst-3342 and Phalloidin-Alexa 647 for 2 h at room temperature. Tissues were washed in PBS and then mounted on glass slides under coverslips in mounting medium (Invitrogen). The slides were left in darkness overnight before observation under a Zeiss LSM900, LSM710 or LSM700 microscope and acquisition with the ZEN software. Three-dimensional reconstructions were performed using the Arivis Vison 4D software.

For microscopy of gut and spleen sections, mice were infected with 5×10^3 CFUs and euthanized at 5 after intravenous inoculation. The intravenous method allowed us to observe only late infection events in the intestine (and not infection events linked to the inoculum as for oral inoculation). Spleen, small intestine and colon were collected without conjunctive tissue, washed in ice-cold PBS and fixed in 4% paraformaldehyde in PBS overnight at 4 °C then washed in PBS, embedded in 4% agarose and sectioned into 70-µm-thick slices using a vibratome. Slices were washed in PBS, then incubated for 2 h in blocking-permeabilization solution (3% bovine serum albumin (BSA) and 0.4% Triton X-100 in PBS). Tissues were then labelled with the appropriate primary antibodies (listed in Supplementary Table 6) overnight at 4 °C in mild blocking conditions (3% BSA and 0.4% Triton X-100 in PBS), washed in PBS, and then incubated with secondary antibodies (listed in Supplementary Table 6), Hoechst-3342 and Phalloidin-Alexa 647 when indicated for 2 h at room temperature. Tissues were washed in PBS and then mounted on glass slides under coverslips in mounting medium. The slides were left in darkness overnight before observation under a Zeiss LSM900 or LM710 microscope and acquisition with the ZEN software. Three-dimensional reconstructions were performed using the Arivis Vison 4D software.

For microscopy of monocytes, sorted monocytes were seeded on poly-D-lysine-coated 96-well-plates or on Nunc Lab-Tek Permanox slides, fixed in 4% paraformaldehyde in PBS overnight at 4 °C and then washed in PBS. Cells were then permeabilized in 0.1% Triton X-100 for 10 min, incubated with blocking solution (5% BSA in PBS) for 30 min at room temperature, then labelled with anti-*Lm* antibody for 1 h at room temperature in PBS-BSA, washed in PBS, and then incubated with anti-rabbit secondary antibody, Hoechst-3342 (Thermo Fisher Scientific) and Phalloidin-Alexa 647 (Thermo Fisher Scientific) for 1 h at room temperature. For total c-Met staining, cells were incubated with anti-c-Met in mild blocking conditions (2.5% BSA, 0.2% Triton X-100 in PBS) overnight at 4 °C, washed in PBS and incubated with anti-*Lm* overnight at 4 °C. For p-AKT and LAMP-1 staining, cells were labelled with primary antibodies solution (anti p-AKT or anti LAMP-1 and anti-*Lm*) in mild blocking conditions (2.5% BSA, 0.2% Triton X-100 in PBS) overnight at 4 °C then washed in PBS. Cells were then incubated with an appropriate solution of secondary antibodies (see Supplementary Table 6) and Hoechst-3342 for 2 h at room temperature, washed in PBS and left in PBS at 4 °C (96-well plates) or covered by mounting medium and a coverslip (Nunc Lab-Tek Permanox slides). For labelling of membrane accessible c-Met, unpermeabilized cells were incubated with blocking solution (5% BSA in PBS) for 30 min at room temperature, then labelled with anti-c-Met in blocking solution without Triton X-100 overnight at 4 °C, washed in PBS and incubated with anti-goat-Alexa 546 in 5% BSA in PBS. Cells were then washed in PBS, permeabilized in 0.1% Triton X-100 and incubated with anti-CD11b in blocking solution (2.5% BSA, 0.2% Triton X-100 in PBS) for 2 h at room temperature, washed in PBS, incubated with anti-rat-Alexa 488 and Hoechst-3342 for 2h at room temperature, washed in PBS and left in PBS at 4 °C (96-well plates) or covered by mounting medium and a coverslip (Nunc Lab-Tek Permanox slides). Cells were observed under a Zeiss LSM900 or LM710 microscope and images acquired with the ZEN software. Three-dimensional reconstructions were performed using the Arivis Vison 4D software.

For microscopy of BHI grown-bacteria, 50 µl of the overnight culture was diluted in 1 ml PBS, spun down in a microfuge for 2 min, fixed in 4% paraformaldehyde in PBS for 15 min at room temperature, then washed in PBS. Bacteria were then permeabilized using 0.5% Triton X-100 for 10 min, washed in PBS, then incubated with blocking solution (1% BSA in PBS) for 30 min. Next, bacteria were labelled with anti-InlB primary antibody in blocking solution (1% BSA in PBS) for 1 h at room temperature, washed three times in PBS, then incubated with anti-rabbit secondary antibody for 1 h at room temperature. After three washes in PBS, bacteria were resuspended in Hoechst solution (dilution 1/5,000 in PBS) for 15 min at room temperature, washed twice with PBS then resuspended in 4 µl PBS. Finally, the bacterial suspension was loaded onto a glass slide coated with 1% agarose gel and a coverslip before observation under a Zeiss LM710 microscope and acquisition with the ZEN software.

Quantification of adhering infected monocytes

For microscopy quantification of infected monocytes adhering to the brain vasculature, mice were inoculated intravenously with high inocula (5×10^5–5×10^6 CFUs) and euthanized after two days, a time point with enough crossing events to allow analysis but without damages to the blood–brain barrier. As mice reach the humane end-point in two days with this high inoculum, to quantify the dynamics of the recruitment of infected monocytes to brain blood vessels when the adaptive immune response starts to act (later than 2 dpi), we inoculated mice first via the intravenous route with 10^3 CFU of GFP-*Lm*, and again two days later with 1×10^6–5×10^6 CFU of tdTomato-*Lm*. This allowed us to induce a high-level infection, which is necessary to detect *Lm*-tdTomato-infected monocytes in the brain vasculature, during a time window (from 2–4 dpi) when the adaptive immune response is developing, and when wild-type-infected monocytes have a lifespan 50% longer than Δ*inlB*-infected ones in mice with a functional adaptive immune system (half-life experiments; Extended Data Fig. 6j). Quantification was performed on a 40-µm-thick medio-sagittal brain section. The number of $Ly6C^+$ infected cells observed adhering to brain blood vessels (visualized by Ly6C and actin staining) on the whole tissue section was quantified. The mean value of two sections per mouse is reported in the figures.

Immunoblotting

To assess the expression level of InlB, bacterial cultures at an $OD_{600\,nm}$ of 0.8 were centrifuged at 3,000*g* for 10 min. Pellets were then incubated with B-PER Complete Bacterial Protein Extraction Reagent (Thermo Fisher Scientific) for 15 min at room temperature and centrifuged at 16,000*g* for 20 min to obtain lysates.

Lysates were mixed with reducing sample buffer (NuPAGE, Invitrogen) for electrophoresis and subsequently transferred onto a nitrocellulose membrane. Membranes were then blocked with 5% non-fat milk diluted in PBS Tween 0.1% for 1 h and incubated with primary antibodies in blocking solution for 2 h at room temperature. After 1 h of incubation with secondary antibodies, immunodetection was performed by using a chemiluminescence kit (Amersham ECL Prime, GE Healthcare), and bands were revealed using the PXi imaging system (Syngene). All uncropped immunoblots are included in Supplementary Fig.1.

In vitro monocyte infection assays

C57BL/6JRj mice were euthanized and bone marrow was collected aseptically. Cells were washed in PBS, red blood cells lysed as described in the flow cytometry section and monocytes isolated using the mouse Monocyte Isolation Kit (Miltenyi Biotec) following the manufacturer's instructions. Cells were incubated overnight at 37 °C in RPMI + 10% FCS and penicillin–streptomycin, washed in RPMI, plated in 96-well plates, infected with GFP-expressing *Lm* at a multiplicity of infection (MOI) of 5 for 1 h at 37 °C and treated with 50 µg ml^{-1} gentamicin for 1 h at 37 °C. For bacterial enumeration, cells were washed in PBS, lysed in 0.1% triton, serially diluted in PBS and plated onto BHI agar. For flow cytometry analysis, cells were washed, fixed in IC fixation buffer in the presence of CountCAL beads, acquired on an X-20 Fortessa SORP apparatus and analysed using FlowJo software.

In vitro infection of Vero cells

Vero cells (ATCC CCL-81) were directly purchased from ATCC, which performed authentication, and were negative for mycoplasma contamination. Vero cells were seeded on poly-D-lysine-coated 96-well plates in DMEM (Invitrogen) + 5% FCS and penicillin–streptomycin 24 h before infection. On the day of infection, cells were washed three times in DMEM + 0.2% FCS and incubated in this medium for four hours.

Bacteria grown in BHI at 37 °C and 200 rpm until $OD_{600\,nm}$ = 0.8 were centrifuged, washed in PBS, suspended in DMEM and added to the cells at a MOI of 50. After 1 min of centrifugation at 200*g*, cells were incubated at 37 °C for the indicated times, fixed for 15 min in 4% PFA and washed three times in PBS. Staining for microscopy was performed as for sorted monocytes in the above section.

Statistical analyses

Analyses were performed using GraphPad Prism 8 software. The numbers of independent experiments performed for the main figures are found in Supplementary Table 7 and in the corresponding legends for the Extended Data figures. Each dot corresponds to one mouse or one sample, unless stated otherwise. All statistical tests were two-sided. All data are presented as median ± interquartile (Fig. 1a, Extended Data Figs. 1c, o, 6j), mean ± s.d. (Figs. 2a, h, 3f–h, j, 4g, Extended Data Figs. 1l, 2a, m–p, r, 5m, n, 6d, f, g, 8b, j), mean (Extended Data Figs. 1p, Fig. 6e, 7b), violin plots (Extended Data Fig. 3f) and as median ± interquartile (box) and extreme values (lines) for all the other data. CFU are compared with the unpaired Mann–Whitney test (two samples) or Kruskal–Wallis test with Dunn's post hoc test (more than two samples). CFU in competition assays are compared with the Wilcoxon matched-pairs signed rank test and competition indexes are compared with the unpaired Mann–Whitney test (two samples) or Kruskal–Wallis test with Dunn's post hoc test (more than two samples). The numbers of infected cells are compared with the unpaired Mann–Whitney test (two samples), Kruskal–Wallis test with Dunn's post hoc test (more than two samples) or Friedman test with Dunn's post-hoc test (Fig. 1c, d, Extended Data Fig. 1d). Expression data (quantitative PCR (qPCR) and flow cytometry) are compared with the unpaired Student's *t*-test (two samples) or one-way ANOVA with Tukey post-hoc test (more than two samples). Growth curves were fitted with a Gompertz model and the lag phases (*k* parameter) for each pair of *Lm* strains were compared with the extra sum-of-squares *F*-test (Extended Data Fig. 2a). Half-lives were compared using the extra-sum of squares *F*-test (Extended Data Fig. 6j). The proportions of cells with different colocalization patterns are compared with a contingency χ_2 test (Extended Data Figs. 1q, 7b, f). NS: $P > 0.05$; $^{*}P < 0.05$, $^{**}P < 0.01$, $^{***}P < 0.001$, $^{****}P < 0.0001$.

Reporting summary

Further information on research design is available in the Nature Research Reporting Summary linked to this paper.

Data availability

The datasets generated and/or analysed during this study are available as Source Data. Source data are provided with this paper.

46. Shinkai, Y. et al. RAG-2-deficient mice lack mature lymphocytes owing to inability to initiate V(D)J rearrangement. *Cell* **68**, 855–867 (1992).
47. Malissen, M. et al. Altered T cell development in mice with a targeted mutation of the CD3-epsilon gene. *EMBO J.* **14**, 4641–4653 (1995).
48. Kitamura, D., Roes, J., Kühn, R. & Rajewsky, K. A B cell-deficient mouse by targeted disruption of the membrane exon of the immunoglobulin μ chain gene. *Nature* **350**, 423–426 (1991).
49. Jung, S. et al. Analysis of fractalkine receptor CX_3CR1 function by targeted deletion and green fluorescent protein reporter gene insertion. *Mol. Cell. Biol.* **20**, 4106–4114 (2000).
50. Hameyer, D. et al. Toxicity of ligand-dependent Cre recombinases and generation of a conditional Cre deleter mouse allowing mosaic recombination in peripheral tissues. *Physiol. Genomics* **31**, 32–41 (2007).
51. Buch, T. et al. A Cre-inducible diphtheria toxin receptor mediates cell lineage ablation after toxin administration. *Nat. Methods* **2**, 419–426 (2005).
52. Matsuzawa, A. et al. A new allele of the lpr locus, lprcg, that complements the gld gene in induction of lymphadenopathy in the mouse. *J. Exp. Med.* **171**, 519–531 (1990).
53. Kägi, D. et al. Cytotoxicity mediated by T cells and natural killer cells is greatly impaired in perforin-deficient mice. *Nature* **369**, 31–37 (1994).
54. Huang, Q. Q. et al. FLIP: a novel regulator of macrophage differentiation and granulocyte homeostasis. *Blood* **116**, 4968–4977 (2010).
55. Huh, C.-G. et al. Hepatocyte growth factor/c-met signaling pathway is required for efficient liver regeneration and repair. *Proc. Natl Acad. Sci. USA* **101**, 4477–4482 (2004).
56. Canli, Ö. et al. Myeloid cell-derived reactive oxygen species induce epithelial mutagenesis. *Cancer Cell* **32**, 869–883 (2017).
57. Monk, I. R., Gahan, C. G. M. & Hill, C. Tools for functional postgenomic analysis of listeria monocytogenes. *Appl. Environ. Microbiol.* **74**, 3921–3934 (2008).
58. Arnaud, M., Chastanet, A. & Débarbouillé, M. New vector for efficient allelic replacement in naturally nontransformable, low-GC-content, Gram-positive bacteria. *Appl. Environ. Microbiol.* **70**, 6887–6891 (2004).
59. Argov, T., Rabinovich, L., Sigal, N. & Herskovits, A. A. An effective counterselection system for *Listeria monocytogenes* and its use to characterize the monocin genomic region of strain 10403S. *Appl. Environ. Microbiol.* **83**, e02927-16 (2017).
60. Balestrino, D. et al. Single-cell techniques using chromosomally tagged fluorescent bacteria to study *Listeria monocytogenes* infection processes. *Appl. Environ. Microbiol.* **76**, 3625–3636 (2010).
61. Quereda, J. J. et al. A dual microscopy-based assay to assess *Listeria monocytogenes* cellular entry and vacuolar escape. *Appl. Environ. Microbiol.* **82**, 211–217 (2016).
62. Disson, O. et al. Modeling human listeriosis in natural and genetically engineered animals. *Nat. Protoc.* **4**, 799–810 (2009).
63. Lu, H. et al. Subcutaneous angiotensin II infusion using osmotic pumps induces aortic aneurysms in mice. *J. Vis. Exp.* **103**, e53191 (2015).

Acknowledgements We thank P. Bousso and A. Fischer for discussions and the members of the Biology of Infection Unit for their support, in particular L. Travier for technical help on brain microscopy and L. Hafner for contributing to data analysis, and the National Reference Center *Listeria*. We thank the Cytometry and Biomarkers Unit of Technology and Service (CB UTechS), the Center for Animal Resources and Research (C2RA) and D. Ershov and J.-Y. Tinevez from the Image Analysis Hub at Institut Pasteur. We are grateful to G. de Saint Basile and F. Sepuvelda for the *Prf1* KO mice, F. Rieux-Laucat for the $Fas^{lpr\text{-}cg}$ mice, R. Pope for the $Flip^{flox/flox}$ mice, F. Greten for the *LysM*-$CreER^{T2}$ mice, A. Eychene for the $Met^{flox/flox}$ mice and J. Pizarro-Cerda and P. Cossart for the pAD β-lactamase plasmid. Figures 1j, 4l and Extended Data Figs. 5l, 9a were created with BioRender. Work in the M.L. laboratory is funded by the Institut Pasteur, Inserm, ERC, ANR, DIM1HEALTH, Labex IBEID (ANR-10-LABX-62-IBEID) and the Fondation Le Roch-Les Mousquetaires. C.M. and M.K. were recipients of the Roux-Cantarini fellowship of the Institut Pasteur. L.H., C.G. and J.G. were supported by the Université de Paris; Y.-H.T. by the Pasteur–Paris University (PPU) International PhD Program under the European Union's Horizon 2020 research and innovation program, Marie Sklodowska-Curie grant agreement no 665807; and S.L. by FRM (ECO201906009119) and 'Ecole Doctorale FIRE-Programme Bettencourt'. M.L. is a member of the Institut Universitaire de France.

Author contributions M.L. initiated and coordinated the study. C.M., M.K., S.L. and M.L. conceived and designed the experimental strategy. C.M. and M.K. performed in vivo and cell sorting for ex vivo experiments. C.M. performed flow cytometry experiments. S.L. and Y.-H.T. performed in vivo experiments and imaging of CNS tissue samples. J.G. performed in vivo experiments and imaging of infected intestinal tissue. O.D. and M.K. did ex vivo monocyte imaging. C.M., L.H. and C.G. designed and performed qPCR with reverse transcription experiments. C.M. and L.H. performed cloning and mutagenesis. M.K. performed western blotting experiments. C.M., M.K., S.L., J.G., O.D., Y.-H.T. and M.L. analysed the data. C.M., S.L. and M.L. wrote the manuscript, M.K. and O.D. edited it and all authors agreed on its final version.

Competing interests The authors declare no competing interests.

Additional information

Supplementary information The online version contains supplementary material available at https://doi.org/10.1038/s41586-022-04505-7.

Correspondence and requests for materials should be addressed to Marc Lecuit.

Peer review information *Nature* thanks Keith Ireton, Junying Yuan and the other, anonymous, reviewer(s) for their contribution to the peer review of this work. Peer reviewer reports are available.

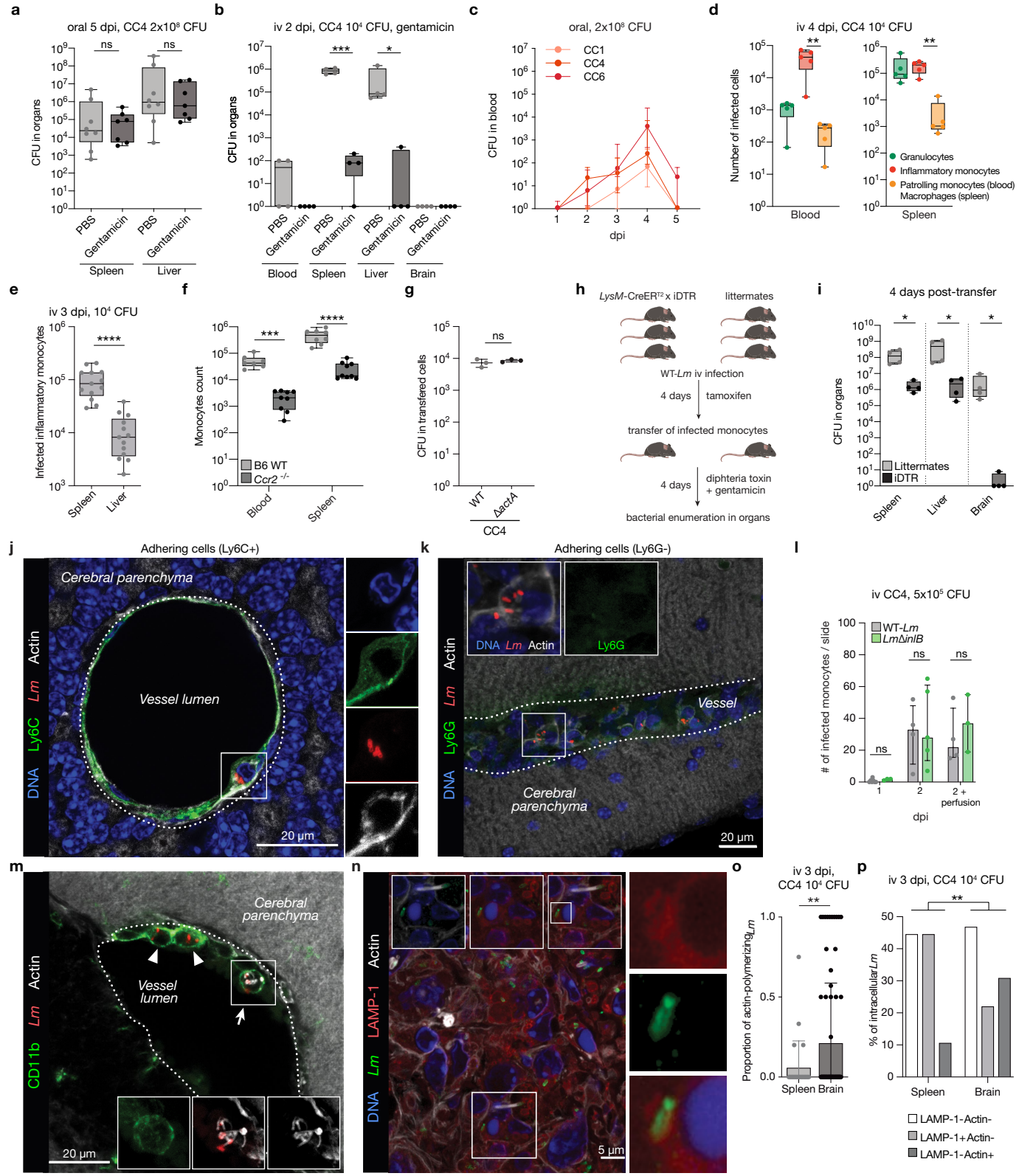

Extended Data Fig. 1 | See next page for caption.

Extended Data Fig. 1 | Infected inflammatory monocytes transfer *Lm* to the brain. (**a**) Bacterial load in the spleen and liver 5 days after oral inoculation with CC4-*Lm*, in mice treated with gentamicin intraperitoneally every day from day 1 post-inoculation, related to Fig. 1b. (**b**) Bacterial load in organs after iv inoculation with CC4-*Lm*, immediately followed by intravenous injection of gentamicin, assessing the bactericidal effect of gentamicin on extracellular circulating *Lm*. (**c**) Bacterial load in the blood after oral inoculation with CC1/CC4/CC6-*Lm*, related to Fig. 1a. (**d**) Repartition of the 3 main infected cell subsets in the blood and spleen after iv inoculation with CC4-*Lm*. (**e**) Number of infected inflammatory monocytes in the spleen and liver of B6-WT mice 3 days after iv inoculation with CC4-*Lm*, showing that monocytes are infected in the spleen by an order of magnitude more than in the liver. (**f**) Number of inflammatory monocytes in the blood and spleen of B6-WT or *Ccr2*$^{-/-}$ mice. (**g**) Number of bacteria in transferred infected monocytes, collected from spleen of mice 3 days after inoculation with CC4, related to Fig. 1f. (**h**) Schematic pipeline of the transfer experiment in *LysM*-CreER^{T2} × iDTR mice. (**i**) Bacterial load in the spleen, liver and brain of gentamicin- and diphtheria toxin-treated recipient *LysM*-CreER$^{T2+/-}$ × *Rosa26*-iDTR$^{+/-}$ and littermate mice, 4 days after injection of infected monocytes collected from infected donor tamoxifen-treated *LysM*-CreER$^{T2+/-}$ × *Rosa26*-iDTR$^{+/-}$ or littermate mice. (**j**, **k**) Representative fluorescence microscopy images of brain sections with infected inflammatory monocytes adhering to endothelial cells after iv inoculation with 5×10^5 CFU CC1-*Lm*. Adhering infected cells are Ly6C$^+$ (j) and Ly6G$^-$ (k). (**l**) Number of infected monocytes adhering to brain blood vessels of mice inoculated with WT-CC4 or CC4Δ*inlB* with or without perfusion of vasculature. (**m**) Representative fluorescence microscopy image of a brain section with infected inflammatory monocytes adhering to endothelial cells after iv inoculation with 5×10^5 CFU CC1-*Lm*. Arrow: *Lm* polymerizing actin in a monocyte; arrowheads: infected monocytes. (**n**) Representative fluorescence microscopy image of splenocytes 5 days after iv inoculation with 10^4 CFU CC4-*Lm*, in which intracellular *Lm* are found polymerizing actin (top insets) or in LAMP-1 positive vacuole (right insets). (**o**, **p**) Proportion of *Lm* detected polymerizing actin in each infected monocyte (o), or overall fraction of *Lm* associated with actin or LAMP-1 vacuoles (p) in monocytes from the spleen or from the blood vasculature of mice after inoculation with CC4-*Lm*. Values in (o) are compared with a *t*-test and proportions in (p) compared with a $\chi 2$ test. Data were obtained from two (a, l) or three (b–h, j–k, m–p) and four (i) independent experiments.

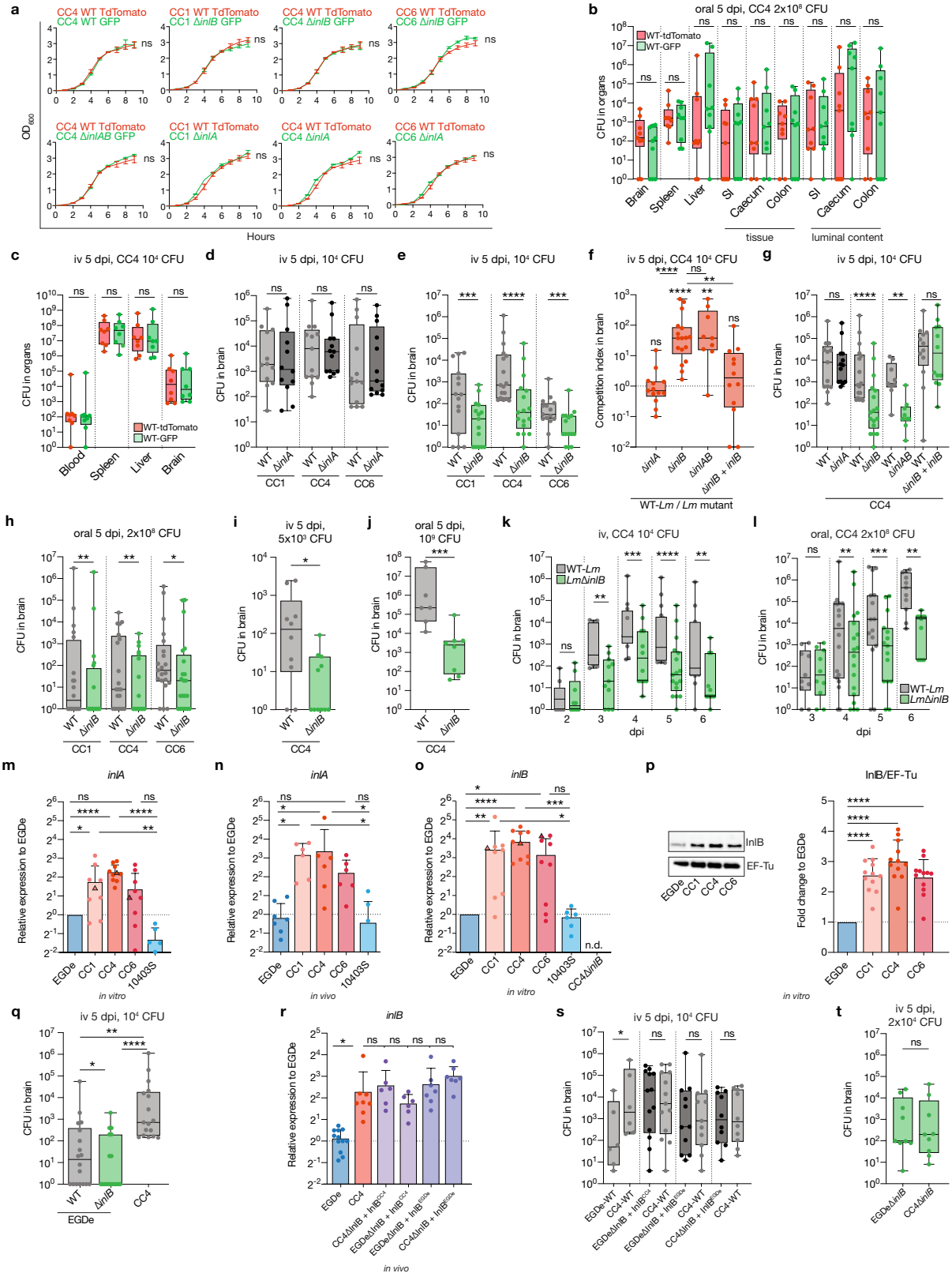

Extended Data Fig. 2 | See next page for caption.

Extended Data Fig. 2 | The expression level of InlB is a major determinant of *Lm* neuroinvasiveness, whereas InlA is not involved. (**a**) Optical density at 600 nm of indicated bacterial strains measured over time after 1:100 dilution in BHI of an overnight culture. (**b**, **c**) Bacterial load after oral inoculation (b) or after iv inoculation (c) with a 1:1 mix of CC4-WT expressing tdTomato or GFP. (**d**) Bacterial load in brain after iv inoculation with a 1:1 mix of WT and Δ*inlA* isogenic strains, related to Fig. 2a. (**e**) Bacterial load in brain after iv inoculation with a 1:1 mix of WT and Δ*inlB* isogenic strains, related to Fig. 2b. (**f**, **g**) Competition indexes (f) and bacterial load (g) in brain after iv inoculation with a 1:1 mix of CC4-WT and either CC4Δ*inlA*, CC4Δ*inlB*, CC4Δ*inlAB* or CC4Δ*inlB* complemented with *inlB* (Δ*inlB* + *inlB*), related to Fig. 2a, b and panels d, e. (**h**) Bacterial load in brain after oral inoculation with a 1:1 mix of WT strain and Δ*inlB* isogenic strains, related to Fig. 2c. (**i**, **j**) Bacterial load in brain after iv inoculation with 5×10^3 CFU (i) or oral inoculation with 10^9 CFU (j) of either CC4-WT or CC4Δ*inlB*. (**k**, **l**) Bacterial load in brain across time after iv inoculation (k) and after oral inoculation (l) with a 1:1 mix of CC4-WT and CC4Δ*inlB*, related to Fig. 2f, g. (**m**) Transcription levels of *inlA* relative to EGDe in mid-log phase in BHI. For CC1/4/6, each dot corresponds to a different clinical isolate and triangles represent the strains used throughout the rest of the study and referred to as CC1, CC4 and CC6, related to panel (o). (**n**) Transcription levels of *inlA* relative to EGDe in infected splenocytes 2 days after iv inoculation with 2×10^5 CFU in mice, related to Fig. 2h. (**o**) Transcription levels of *inlB* relative to EGDe in mid-log phase in BHI. Each dot for CC1/4/6 corresponds to a different clinical isolate and triangles point out the strains used throughout the rest of the study and referred to as CC1, CC4 and CC6. (**p**) Representative Western blot (left) and quantification (right) of InlB expression, normalized to that of EF-Tu, relative to EGDe in mid-log phase in BHI. (**q**) Bacterial load in brain after inoculation with either WT-EGDe, EGDeΔ*inlB* and WT-CC4. (**r**) Transcription levels of *inlB*, relative to EGDe, in infected splenocytes 2 days after iv inoculation with 2×10^5 CFU of EGDe-WT, CC4-WT and strains complemented with either *inlB* from EGDe or from CC4. (**s**) Bacterial load in brain after inoculation with a 1:1 mix of the indicated bacterial strains, related to Fig. 2i. (**t**) Bacterial load in brain after inoculation with a 1:1 mix of EGDe*ΔinlB* and CC4*ΔinlB*, related to Fig. 2i. Data were obtained from three independent experiments.

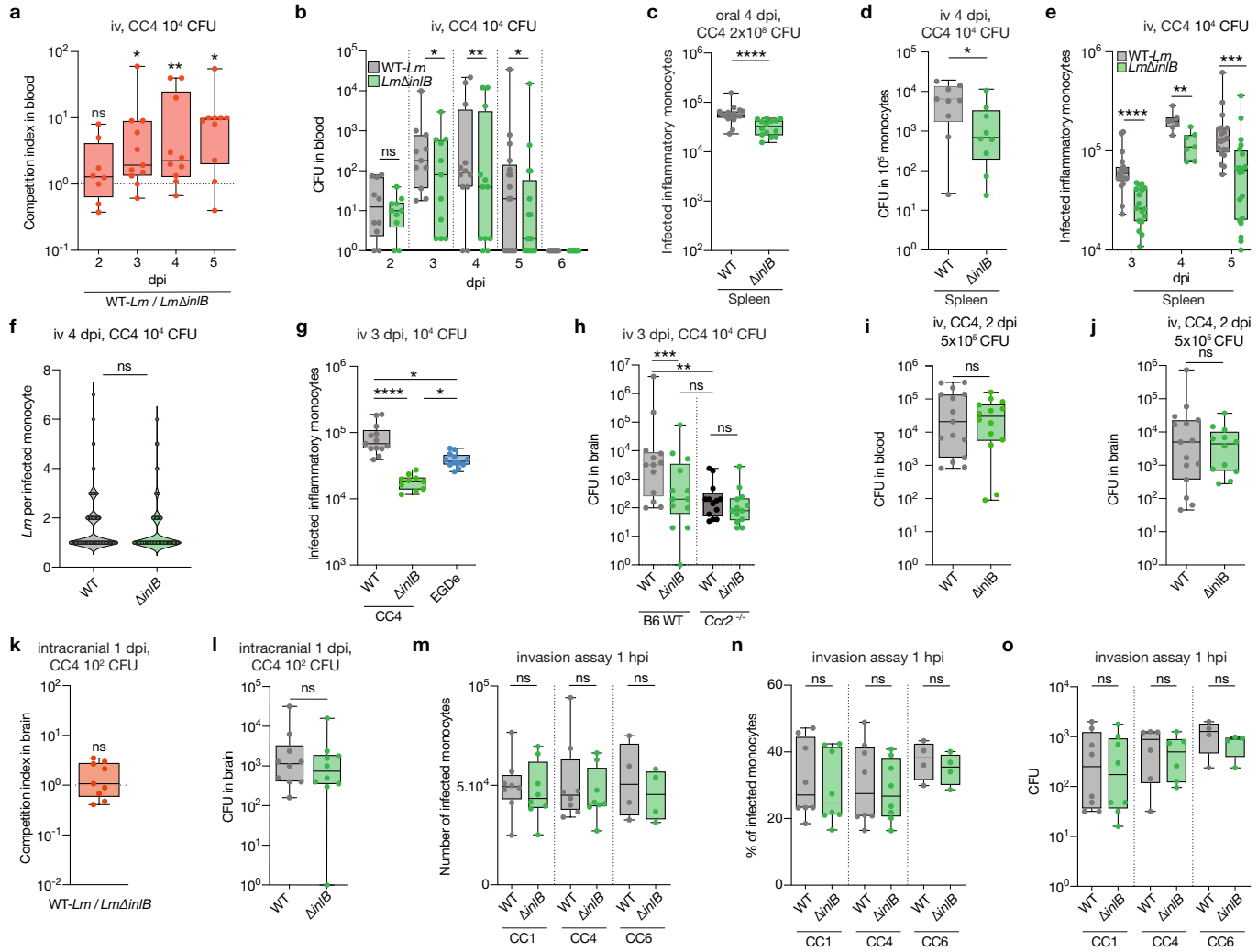

Extended Data Fig. 3 | InlB is not involved in *Lm* invasion of monocytes. (**a**, **b**) Competition indexes (a) and bacterial load (b) in blood after iv inoculation with a 1:1 mix of CC4-WT and CC4Δ*inlB*. (**c**) Number of infected monocytes in the spleen after inoculation with CC4-WT or CC4*ΔinlB*. (**d**) Bacterial load from 10^5 sorted monocytes (infected or not) retrieved from mice after inoculation with CC4-WT or CC4Δ*inlB*. (**e**) Number of infected monocytes across time in the spleen after inoculation with either CC4-WT or CC4Δ*inlB*. (**f**) Number of bacteria per infected monocyte collected from mice after inoculation with either CC4-WT or CC4Δ*inlB*. (**g**) Number of infected monocytes in the spleen after inoculation with CC4-WT, CC4Δ*inlB* or EGDe-WT. (**h**) Bacterial load in brain of B6-WT or *Ccr2*$^{-/-}$ mice after inoculation with a 1:1 mix of CC4-WT and CC4Δ*inlB*, related to Fig. 2l. (**i**, **j**) Bacterial load in blood (i) and brain (j) after iv inoculation with 5×10^5 CFU of either CC4-WT or CC4Δ*inlB*. (**k**, **l**) Competition index (k) and bacterial load (l) in brain 1 day after intracranial inoculation with a 1:1 mix of CC4-WT and CC4Δ*inlB*. (**m**-**o**) Number of infected monocytes (m), percentage of infected monocytes (n) and bacterial load (o) in monocytes 1 h after *in vitro* infection of primary bone marrow mouse monocytes with WT-Lm or Δ*inlB* isogenic mutants, at a MOI of 5. Data were obtained from two (k–l), three (a–j) and four (m–o) independent experiments.

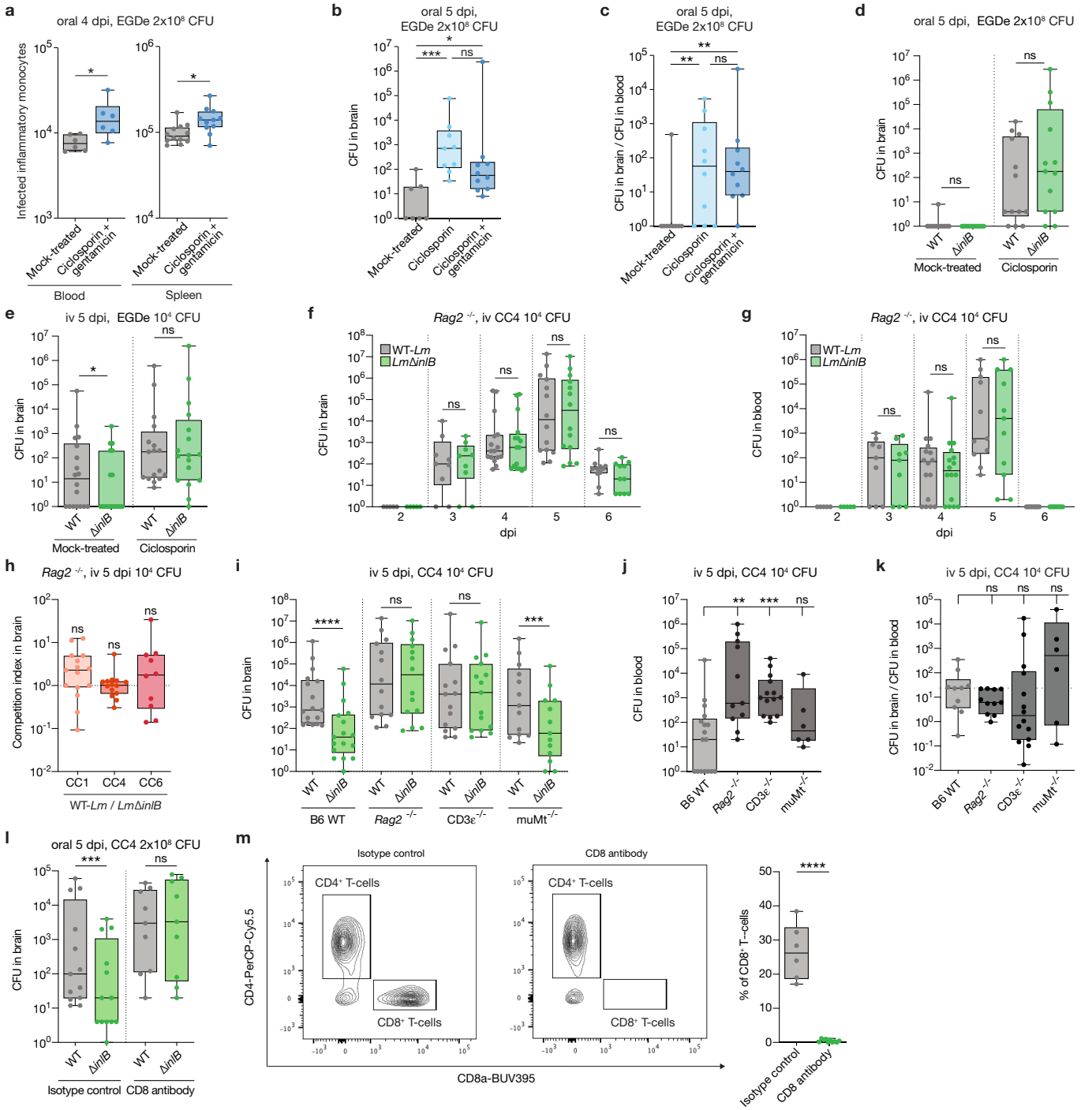

Extended Data Fig. 4 | *Lm* neuroinvasion depends on InlB only in the presence of functional CD8⁺ T cells. (**a**) Number of infected monocytes in the blood and spleen of ciclosporin and gentamicin-treated mice after oral inoculation with EGDe. (**b**, **c**) Bacterial load in brain (b) and ratio of brain/blood bacterial load (c) in ciclosporin ± gentamicin-treated mice after oral inoculation with EGDe. (**d**, **e**) Bacterial load in brain of ciclosporin-treated mice after oral (d) and iv (e) inoculation with a 1:1 mix of EGDe-WT and EGDeΔ*inlB*. (**f**, **g**) Bacterial load in brain (f) and in blood (g) of *Rag2*$^{-/-}$ mice after inoculation with a 1:1 mix of CC4-WT and CC4Δ*inlB*, related to Fig. 3f. (**h**) Competition indexes in brain of *Rag2*$^{-/-}$ mice after inoculation with a 1:1 mix of WT strain and Δ*inlB* isogenic strains. (**i**, **j**) Bacterial load in brain (f) and in blood (g) after inoculation with a 1:1 mix of CC4-WT and CC4Δ*inlB* in control B6 WT mice and in mice lacking functional T (CD3ε$^{-/-}$), B lymphocytes (muMt$^{-/-}$) or both (*Rag2*$^{-/-}$), related to Fig. 3d. (**k**) Ratio of brain/blood bacterial loads in B6 WT, *Rag2*$^{-/-}$, CD3ε$^{-/-}$ and muMt$^{-/-}$ mice, related to Fig. 3d. (**l**) Bacterial load in brain of mice after inoculation with a 1:1 mix of CC4-WT and CC4Δ*inlB* after CD8⁺ T cells depletion, related to Fig. 3e. (**m**) Representative dot plots (left) and proportion of CD8⁺ T cells (right) among CD45⁺ CD3⁺ cells in the spleen, after CD8⁺ T cells depletion, related to Fig. 3e. Data were obtained from two (m) or three independent experiments.

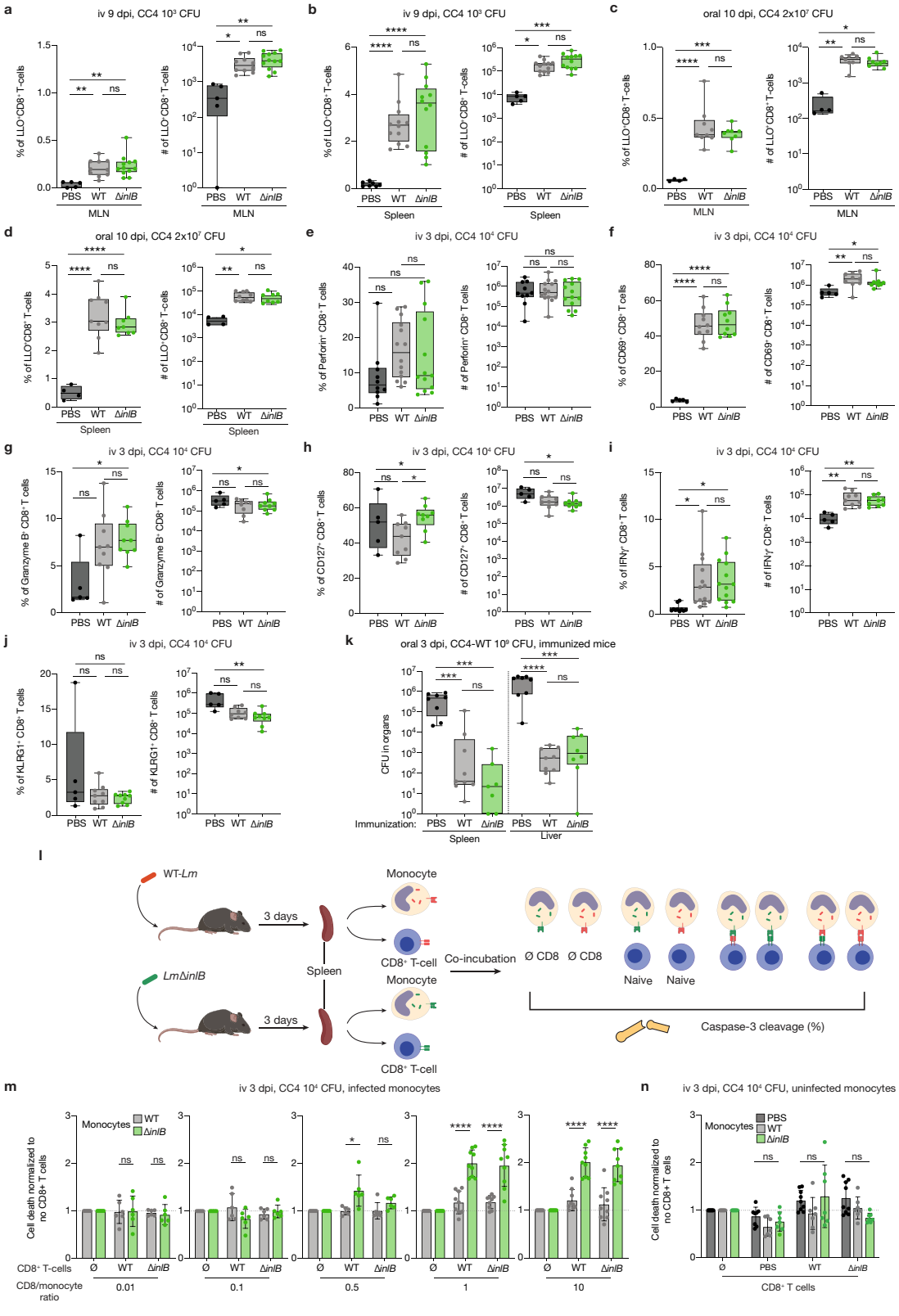

Extended Data Fig. 5 | See next page for caption.

Extended Data Fig. 5 | InlB does not alter the induction and differentiation of specific anti-*Lm* CD8$^+$ T cells. (**a**, **b**) Percentage (left) and number (right) of LLO-specific CD8$^+$ T cells in mesenteric lymph nodes (MLN) (a) and spleen (b) of BALB/c mice after iv inoculation with CC4-WT strain or CC4Δ*inlB*. (**c**, **d**) Percentage (left) and number (right) of LLO-specific CD8$^+$ T cells in MLN (c) and spleen (d) of iFABP-hEcad mice after oral inoculation with CC4-WT strain or CC4Δ*inlB*. (**e**–**j**) Percentage (left) and number (right) of Perforin$^+$ (e), CD69$^+$ (f), Granzyme-B$^+$ (g), CD127$^+$ (h), IFNγ$^+$ (i) and KLRG1$^+$ (j) CD8$^+$ T cells after iv inoculation with CC4-WT or CC4Δ*inlB*. (**k**) Bacterial load in spleen and liver after oral inoculation with CC4-WT in mice challenged 30 days before with $5x10^7$ CFU of CC4-WT or CC4Δ*inlB*. (**l**) Schematic pipeline of the cytotoxic lymphocyte (CTL) assay. (**m**) Level of caspase-3 cleavage of infected spleen monocytes, collected after iv inoculation with CC4-WT or CC4Δ*inlB*, and incubated with CD8$^+$ T cells from similarly infected (WT and Δ*inlB*) or control (PBS) mice at the indicated effector to target ratio, related to Fig. 3i. Results are normalized to the level of caspase-3 cleavage in absence of CD8$^+$ T cells. (**n**) Level of caspase-3 cleavage of uninfected spleen monocytes, collected after iv inoculation with CC4-WT or CC4Δ*inlB*, and incubated with CD8$^+$ T cells from similarly infected (WT and Δ*inlB*) or control (PBS) mice at an effector to target ratio of 5, related to Fig. 3i. Results are normalized to the level of caspase-3 cleavage in absence of CD8$^+$ T cells. Data were obtained from three independent experiments.

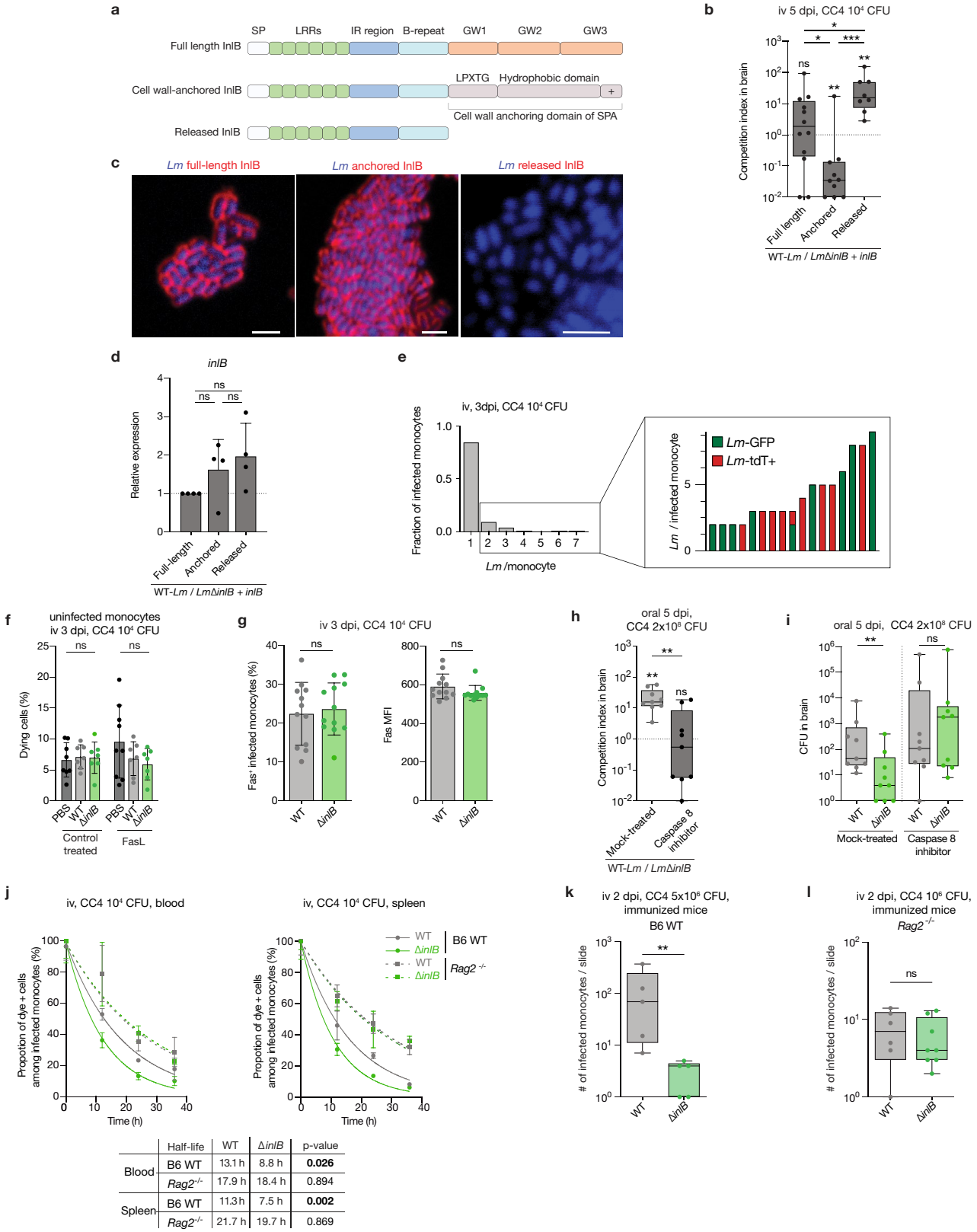

	Half-life	WT	ΔinlB	p-value
Blood	B6 WT	13.1 h	8.8 h	**0.026**
	Rag2$^{-/-}$	17.9 h	18.4 h	0.894
Spleen	B6 WT	11.3 h	7.5 h	**0.002**
	Rag2$^{-/-}$	21.7 h	19.7 h	0.869

Extended Data Fig. 6 | See next page for caption.

Extended Data Fig. 6 | Membrane-associated InlB protects infected monocytes from CD8$^+$ T cell-mediated cell death and increases their lifespan, favouring their adhesion to blood brain vessels. (**a**) Schematic representation of WT (full length) InlB and its anchored and released variants. (**b**) Competition indexes in the brain of mice after inoculation with a 1:1 mix of CC4-WT and CC4Δ*inlB* transformed with a plasmid expressing either full-length WT InlB, cell wall-anchored InlB or released InlB. (**c**) Representative fluorescence microscopy images of centrifugated CC4Δ*inlB* transformed with a plasmid expressing either full length InlB (left panel), anchored InlB (central panel) or released InlB (right panel). Scale bars: 5 µm. (**d**) Transcription level of *inlB* in CC4Δ*inlB* transformed with a plasmid expressing InlB variants in mid-log phase in BHI, relative to CC4Δ*inlB* expressing full length InlB. (**e**) Proportion of infected monocytes containing 1 to 7 bacteria. For monocytes containing more than 1 bacteria, number of GFP- or tdTomato-expressing bacteria in each monocyte is shown. Monocytes were collected 3 days after inoculation with a 1:1 mix of CC4-WT expressing GFP or tdTomato. (**f**) Level of caspase-3 cleavage of non-infected spleen monocytes, collected from mice infected for 3 days with CC4-WT or CC4Δ*inlB*, incubated *ex vivo* with FasL, related to Fig. 3m. (**g**) Percentage of infected spleen monocytes expressing Fas at their surface (left), and the mean fluorescence intensity (MFI) of Fas signal (right), after inoculation with CC4-WT or CC4Δ*inlB*. (**h**, **i**) Competition indexes (h) and bacterial load (i) in brain after inoculation with a 1:1 mix of CC4-WT and CC4Δ*inlB* and treatment with caspase-8 inhibitor. (**j**) Proportion of dye-positive transferred monocytes among infected monocytes in the blood and the spleen after inoculation of B6 WT mice (plain lines) or *Rag2*$^{-/-}$ (dotted lines) with CC4-WT or CC4Δ*inlB*. Calculated half-lives of infected monocytes are shown in the table. (**k**) Number of infected monocytes adhering to brain vessels 2 days after inoculation with 5×10^6 CFU of CC4-WT or CC4Δ*inlB*, expressing tdTomato, of B6 WT mice immunized 2 days before with 10^3 CFU of CC4-WT expressing GFP. Each dot corresponds to the average number of monocytes counted on two slides (representative median sagittal sections, 40 µm thickness) for one mouse. (**l**) Number of infected monocytes adhering to brain vessels 2 days after inoculation with 10^6 CFU of CC4-WT and CC4ΔinlB, expressing tdTomato, of *Rag2*$^{-/-}$ mice immunized 2 days before with 10^3 CFU of CC4-WT expressing GFP. Each dot corresponds to the average number of monocytes counted on two slides (representative median sagittal sections, 40 µm thickness) for one mouse. Data were obtained from two (k, l) or three independent experiments.

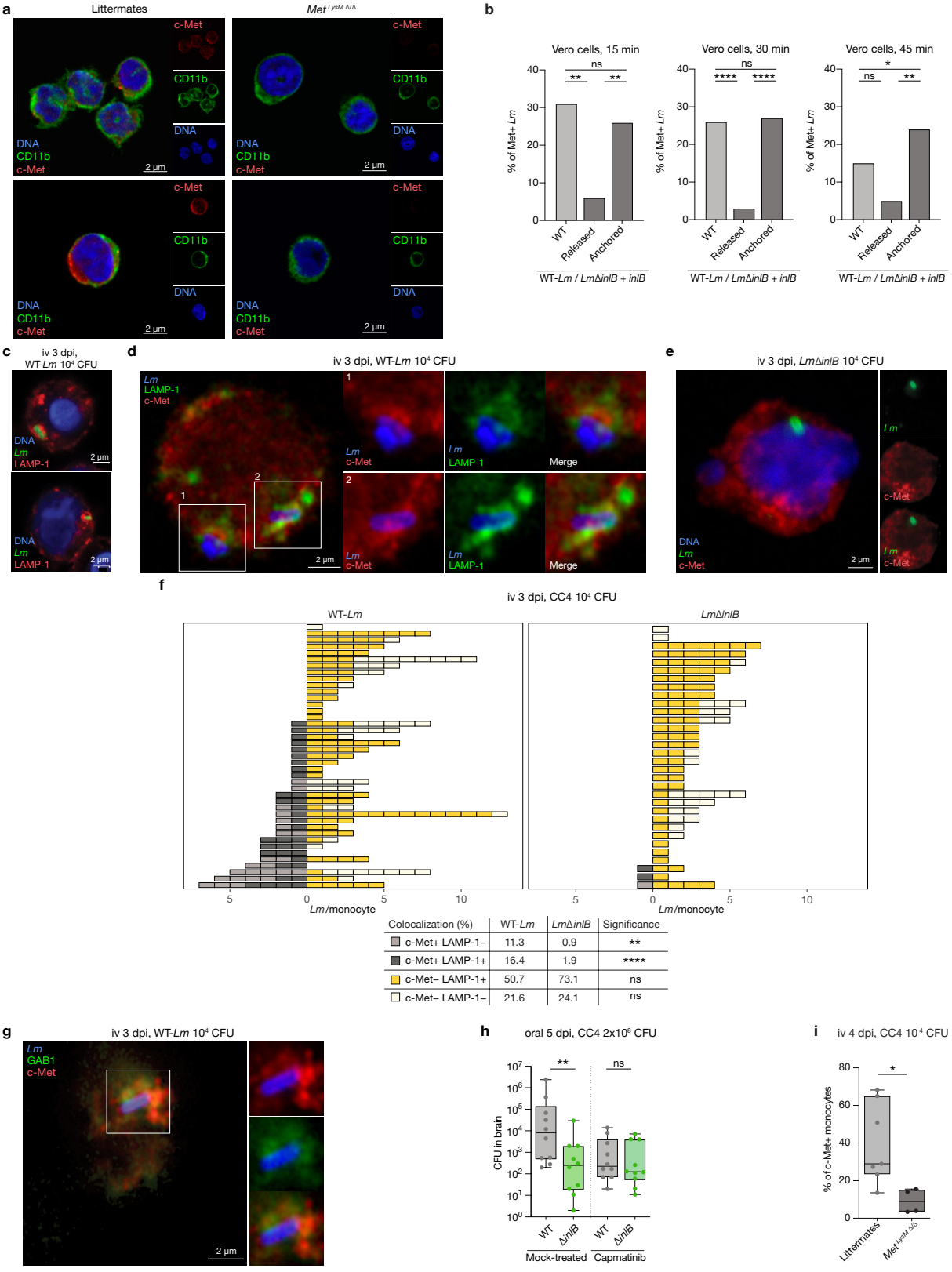

Extended Data Fig. 7 | See next page for caption.

Extended Data Fig. 7 | InlB recruits c-Met in LAMP-1^{+} vacuoles in infected monocytes. (**a**) Representative fluorescence microscopy images of spleen monocytes (not permeabilized) collected from tamoxifen-treated *LysM*-CreER^{T2} × *Met*$^{flox/flox}$ (*Met*$^{LysMΔ/Δ}$) and their littermates, showing specific surface expression of c-Met. (**b**) Percentage of *Lm* co-localizing with c-Met *in vitro* in Vero cells 15 min (left), 30 min (middle) and 45 min (right) after infection at MOI 50 with CC4Δ*inlB* expressing either WT InlB, released InlB or cell wall-anchored InlB. (**c**, **d**) Representative fluorescence microscopy images of spleen monocytes collected after inoculation with CC4-WT, showing intra-vacuolar *Lm* surrounded with LAMP-1 (c) and co-localizing with both c-Met and LAMP-1 (d) related to Supplementary Video 4. (**e**) Representative fluorescence microscopy images of spleen monocytes collected after inoculation with CC4Δ*inlB*, showing no-colocalization with c-Met. (c–e) Maximum intensity projection over a *z*-stack. (**f**) Quantification of intracellular *Lm* co-localizing or not with c-Met and LAMP-1 in infected spleen monocytes collected after inoculation with CC4-WT or CC4Δ*inlB*. Individual cells are plotted in top panel and samples are compared in bottom panel. (**g**) Representative fluorescence microscopy images of spleen monocytes collected after inoculation with CC4-WT, co-localizing with both c-Met and GAB1 related to Supplementary Video 5. Maximum intensity projection over a *z*-stack. (**h**) Bacterial load in brain after inoculation with a 1:1 mix of CC4-WT and CC4Δ*inlB* in mice treated with capmatinib, related to Fig. 4a. (**i**) Proportion of infected spleen monocytes positive for c-Met signal in flow cytometry after inoculation of *Met*$^{LysMΔ/Δ}$ mice and their littermates with CC4-WT. Data were obtained from three independent experiments (a, h and i) or from three microscopic field of views (f).

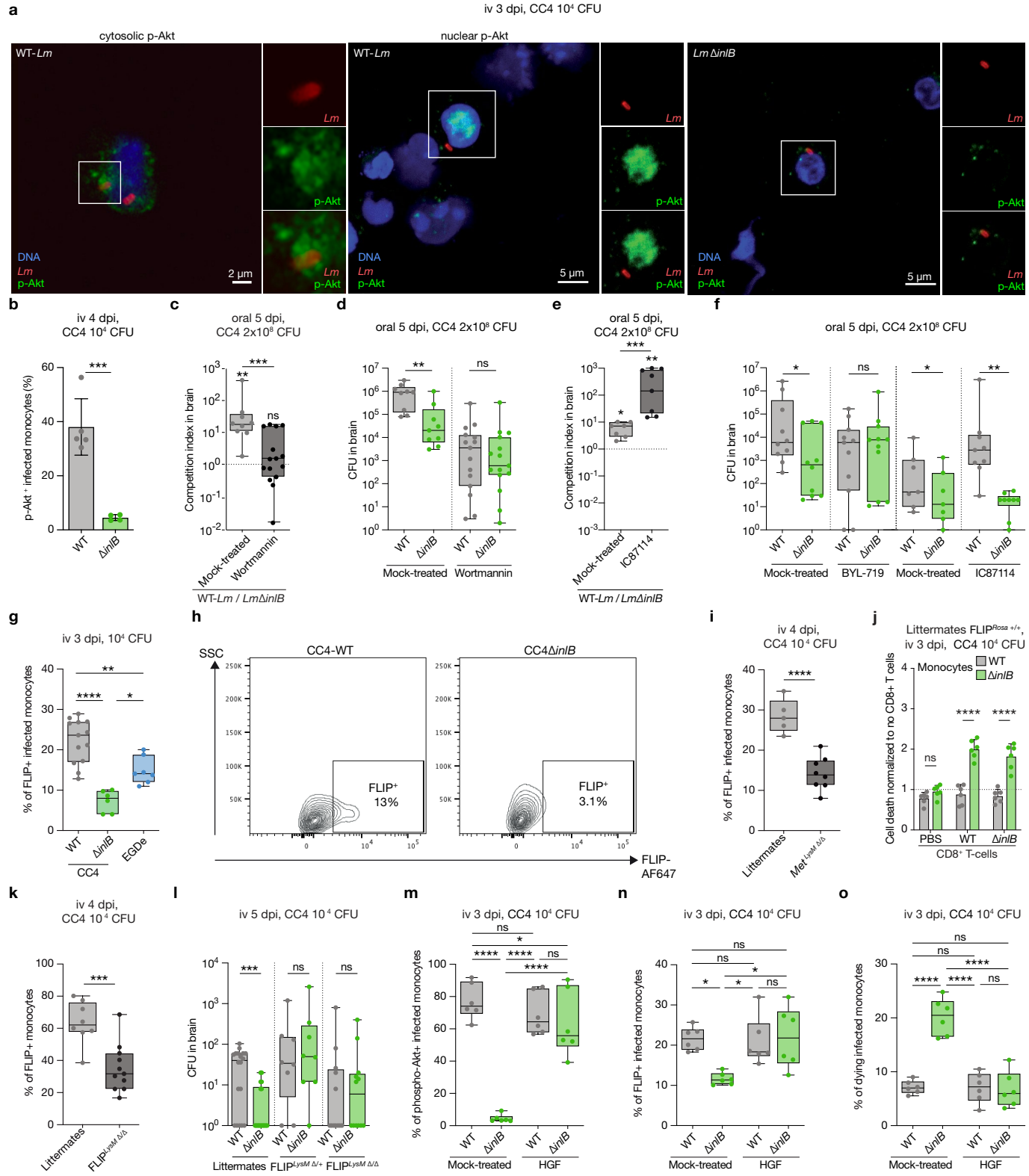

Extended Data Fig. 8 | See next page for caption.

Extended Data Fig. 8 | InlB-mediated neuroinvasion involves the c-Met–PI3Kα–FLIP pathway in infected monocytes. (**a**) Representative fluorescence microscopy images of spleen monocytes collected after inoculation with CC4-WT or CC4Δ*inlB*, showing cytosolic and nuclear phosphorylation of AKT, related to Supplementary Video 6. Images are maximum intensity projection over a *z*-stack. (**b**) Proportion of infected spleen monocytes positive for phospho-AKT signal in flow cytometry after inoculation with CC4-WT or CC4Δ*inlB*. (**c**, **d**) Competition indexes (c) and bacterial load (d) in brain after inoculation with a 1:1 mix of CC4-WT and CC4Δ*inlB* in mice treated with wortmannin. (**e**) Competition indexes in brain after inoculation with a 1:1 mix of CC4-WT and CC4Δ*inlB* in mice treated with PI3Kδ inhibitor (IC87114). (**f**) Bacterial load in the brain after inoculation with a 1:1 mix of CC4-WT and CC4Δ*inlB* in mice treated with BYL-719 or IC87114, related to Fig. 4d and to panel **e**. (**g**) Proportion of infected spleen monocytes positive for FLIP signal in flow cytometry after inoculation with CC4-WT, CC4Δ*inlB* or EGDe-WT. (**h**) Representative dot plot of FLIP expression in infected inflammatory spleen monocytes, after inoculation with CC4-WT or CC4Δ*inlB*, related to Fig. 4e. (**i**) Proportion of infected spleen monocytes positive for FLIP signal in flow cytometry after inoculation with CC4-WT of $Met^{LysM\Delta/\Delta}$ mice and their littermates after tamoxifen treatment. (**j**) Level of caspase-3 cleavage of infected spleen monocytes, collected 3 days after inoculation with CC4-WT or CC4Δ*inlB* of tamoxifen-treated *Rosa26*-CreER^{T2} × $Cflar^{+/+}$ ($Flip^{Rosa+/+}$) littermate mice and incubated with CD8$^+$ T cells from similarly infected mice at an effector to target ratio of 5, related to Fig. 4g. (**k**) Proportion of infected spleen monocytes positive for FLIP signal in flow cytometry, after inoculation with CC4-WT of tamoxifen-treated *LysM*-CreER^{T2} × $Cflar^{flox/flox}$ ($Flip^{LysM\Delta/\Delta}$) mice and their littermates ($Flip^{LysM+/+}$), and after tamoxifen treatment. (**l**) Bacterial load in tamoxifen-treated ($Flip^{LysM\Delta/\Delta}$), *LysM*-CreER^{T2} × $Cflar^{flox/+}$ ($Flip^{LysM\Delta/+}$) and their littermates, after inoculation with a 1:1 mix of CC4-WT and CC4Δ*inlB* and tamoxifen treatment, related to Fig. 4h. Of note, only female mice were used for $Flip^{LysM\Delta/+}$, whereas both male and female mice were included for $Flip^{LysM\Delta/\Delta}$ and their littermates. (**m**–**o**) Proportion of infected spleen monocytes positive for phospho-AKT signal (m), FLIP signal (n) and Zombie signal (o) in flow cytometry, after inoculation with CC4-WT or CC4Δ*inlB* and treatment with HGF. Data were obtained from two (m–o) or three independent experiments.

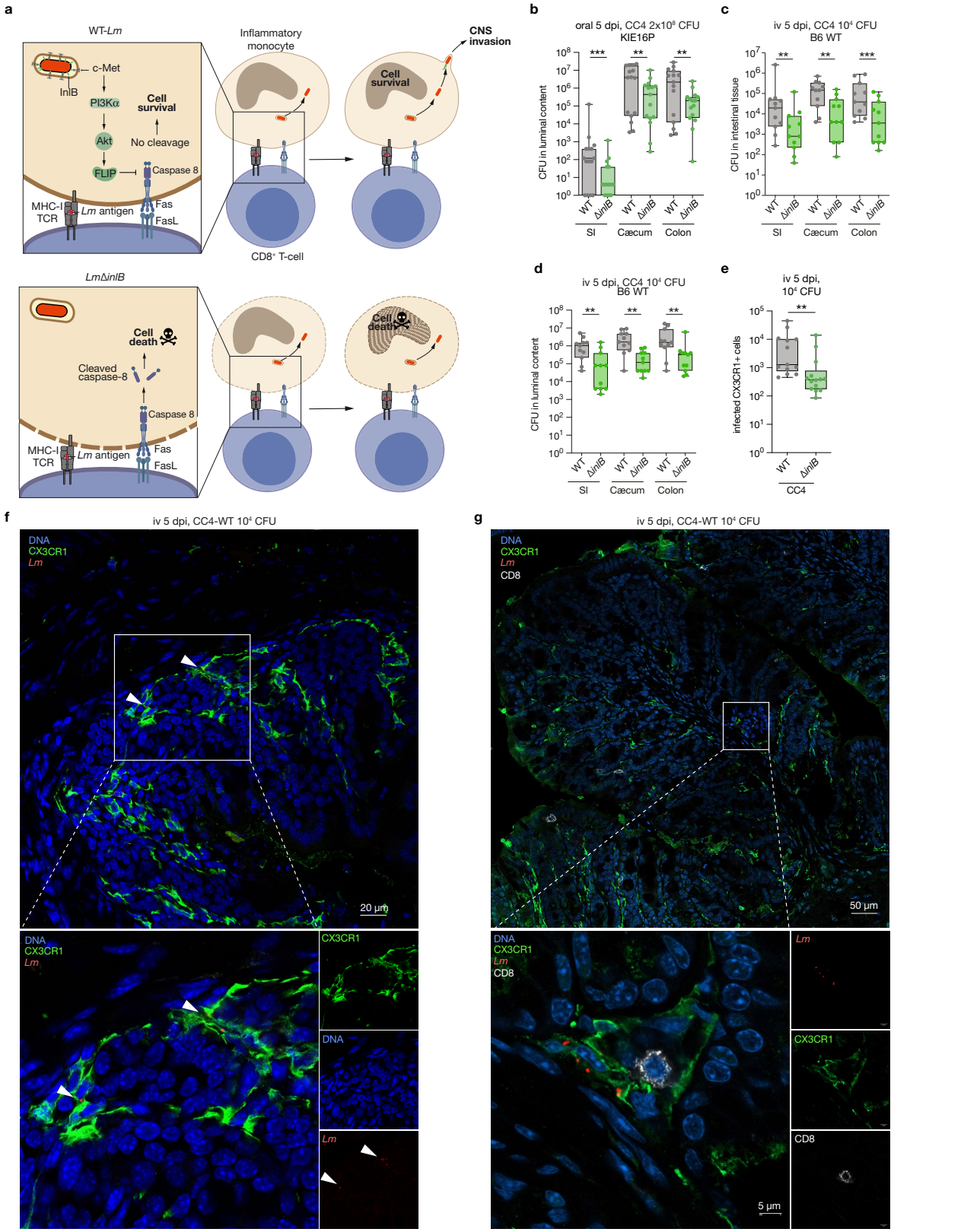

Extended Data Fig. 9 | In the intestinal tract, *Lm* infects CX3CR1$^+$ macrophages of the lamina propria, in an InlB-dependent manner. (**a**) Representation of InlB-activated pathway of infected monocytes survival to Fas-mediated cell death. (**b**–**d**) Bacterial load in luminal content of KIE16P (b) and B6 WT (d) or intestinal tissue of B6 WT (c) mice after oral (b) and iv (c, d) inoculation with a 1:1 mix of CC4-WT and CC4ΔinlB, related to Fig. 4j, k, Extended Data Fig. 10a, c, e, g. (**e**) Number of infected CD11b$^+$ CX3CR1$^+$ macrophages of the lamina propria of the small intestine of B6 WT mice in flow cytometry after inoculation with CC4-WT or CC4Δ*inlB*. (**f**, **g**) Representative fluorescence microscopy images of infected CX3CR1$^+$ infected macrophages in the colon lamina propria of mice after inoculation with CC4-WT, related to Supplementary Videos 7, 8. Data were obtained from three independent experiments. SI = small intestine.

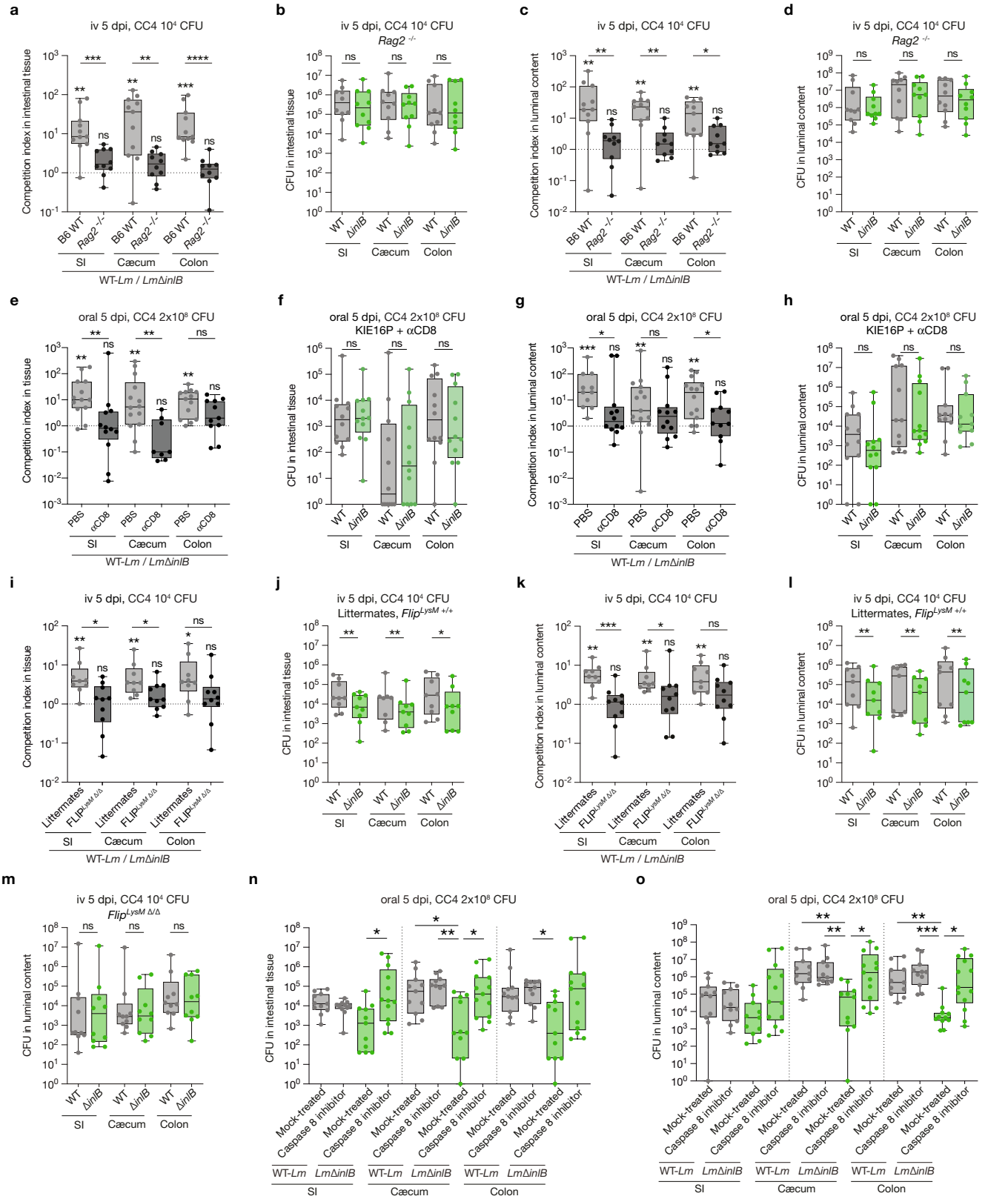

Extended Data Fig. 10 | See next page for caption.

Extended Data Fig. 10 | InlB-mediated *Lm* gut persistence involves resistance to CD8$^+$ T cells and FLIP expression in myeloid cells. (**a**) Competition indexes in intestinal tissue of B6 WT and *Rag2*$^{-/-}$ mice after inoculation with a 1:1 mix of CC4-WT and CC4Δ*inlB*, related to Extended Data Figs. 9c, d and to panels **b**–**d**. (**b**) Bacterial load in intestinal tissue of *Rag2*$^{-/-}$ mice after inoculation with a 1:1 mix of CC4-WT and CC4Δ*inlB*, related to **a**, **c**, **d**. (**c**) Competition indexes in luminal content of B6 WT and *Rag2*$^{-/-}$ mice after inoculation with a 1:1 mix of CC4-WT and CC4Δ*inlB*, related to Extended Data Fig. 9c, d and to panels **a**, **b**, **d**. (**d**) Bacterial load in luminal content of *Rag2*$^{-/-}$ mice after inoculation with a 1:1 mix of CC4-WT and CC4Δ*inlB*, related to panels **a**–**c**. (**e**) Competition indexes in intestinal tissue of mice after inoculation with a 1:1 mix of CC4-WT and CC4Δ*inlB* and treated with an anti-CD8$^+$ T cells antibody, related to Extended Data Fig. 9d and to panels **f**–**h**. (**f**) Bacterial load in intestinal tissue of mice after inoculation with a 1:1 mix of CC4-WT and CC4Δ*inlB* and treated with an anti-CD8$^+$ T cells antibody, related to **e**–**h**. (**g**) Competition indexes in luminal content of mice after inoculation with a 1:1 mix of CC4-WT and CC4Δ*inlB* and treated with an anti-CD8$^+$ T cells antibody, related to Fig. 4j, Extended Data Fig. 9b and to panels **e**–**h**. (**h**) Bacterial load in luminal content of mice after inoculation with a 1:1 mix of CC4-WT and CC4Δ*inlB* and treated with an anti-CD8$^+$ T cells antibody, related to **e**–**g**. (**i**) Competition indexes in intestinal tissue of *Flip*$^{LysMΔ/Δ}$ mice and their littermates after inoculation with a 1:1 mix of CC4-WT and CC4Δ*inlB*, related to Fig. 4k and to panels **j**–**m**. (**j**) Bacterial load in intestinal tissue of littermates of *Flip*$^{LysMΔ/Δ}$ mice after inoculation with a 1:1 mix of CC4-WT and CC4Δ*inlB*, related to Fig. 4k and to panels **i**, **k**–**m**. (**k**) Competition indexes in luminal content of *Flip*$^{LysMΔ/Δ}$ mice and their littermates after inoculation with a 1:1 mix of CC4-WT and CC4Δ*inlB*, related to Fig. 4k and to panels **i**, **j**, **l**, **m**. (**l**) Bacterial load in luminal content of littermates of *Flip*$^{LysMΔ/Δ}$ mice after inoculation with a 1:1 mix of CC4-WT and CC4Δ*inlB*, related to Fig. 4k and to panels **i**–**k**, **m**. (**m**) Bacterial load in luminal content of *Flip*$^{LysMΔ/Δ}$ mice after inoculation with a 1:1 mix of CC4-WT and CC4Δ*inlB*, related to Fig. 4k and to panels **i**–**l**. (**n**, **o**) Bacterial load in intestinal tissue (n) and luminal content (o) of mice after inoculation with either CC4-WT or CC4Δ*inlB* and treated with caspase-8 inhibitor, related to Fig. 3k. Data were obtained from three independent experiments. SI = small intestine.

nature research

Corresponding author(s): Marc Lecuit

Last updated by author(s): Dec 2, 2021

Reporting Summary

Nature Research wishes to improve the reproducibility of the work that we publish. This form provides structure for consistency and transparency in reporting. For further information on Nature Research policies, see our Editorial Policies and the Editorial Policy Checklist.

Statistics

For all statistical analyses, confirm that the following items are present in the figure legend, table legend, main text, or Methods section.

n/a	Confirmed
☐	☒ The exact sample size (*n*) for each experimental group/condition, given as a discrete number and unit of measurement
☐	☒ A statement on whether measurements were taken from distinct samples or whether the same sample was measured repeatedly
☐	☒ The statistical test(s) used AND whether they are one- or two-sided *Only common tests should be described solely by name; describe more complex techniques in the Methods section.*
☒	☐ A description of all covariates tested
☐	☒ A description of any assumptions or corrections, such as tests of normality and adjustment for multiple comparisons
☐	☒ A full description of the statistical parameters including central tendency (e.g. means) or other basic estimates (e.g. regression coefficient) AND variation (e.g. standard deviation) or associated estimates of uncertainty (e.g. confidence intervals)
☐	☒ For null hypothesis testing, the test statistic (e.g. *F*, *t*, *r*) with confidence intervals, effect sizes, degrees of freedom and *P* value noted *Give P values as exact values whenever suitable.*
☒	☐ For Bayesian analysis, information on the choice of priors and Markov chain Monte Carlo settings
☒	☐ For hierarchical and complex designs, identification of the appropriate level for tests and full reporting of outcomes
☒	☐ Estimates of effect sizes (e.g. Cohen's *d*, Pearson's *r*), indicating how they were calculated

Our web collection on statistics for biologists contains articles on many of the points above.

Software and code

Policy information about availability of computer code

Data collection	Confocal microscopy data were acquired using ZEN Black v2.3 or ZEN Blue v3.2 Cytometry data were acquired using BD FACSDiva v8.0.1
Data analysis	Flow cytometry data were analyzed using FlowJo v10 3D reconstruction of microscopy was performed using Arivis Vision 4D v3.0 Data analysis was performed with Graphpad Prism v8.0-9.0

For manuscripts utilizing custom algorithms or software that are central to the research but not yet described in published literature, software must be made available to editors and reviewers. We strongly encourage code deposition in a community repository (e.g. GitHub). See the Nature Research guidelines for submitting code & software for further information.

Data

Policy information about availability of data

All manuscripts must include a data availability statement. This statement should provide the following information, where applicable:

- Accession codes, unique identifiers, or web links for publicly available datasets
- A list of figures that have associated raw data
- A description of any restrictions on data availability

All datasets generated during and/or analysed during the current study are available as Source Data attached to this manuscript.

Field-specific reporting

Please select the one below that is the best fit for your research. If you are not sure, read the appropriate sections before making your selection.

☒ Life sciences ☐ Behavioural & social sciences ☐ Ecological, evolutionary & environmental sciences

For a reference copy of the document with all sections, see nature.com/documents/nr-reporting-summary-flat.pdf

Life sciences study design

All studies must disclose on these points even when the disclosure is negative.

Sample size	No sample size calculations were performed. The sample size (n) of each experiment is provided in each panel as each dot corresponds to one mouse/sample. Sample sizes were chosen to support meaningful conclusions with the statistical tests used. We used around 8 to 14 mice per group, a number sufficient to reach statistical significance using non-parametric statistical tests with the effect size we expected to observe, based on our previous observations.
Data exclusions	No data were excluded, except when mice reached ethical endpoints before the pre-determined timepoints of killing: they were terminated early without being included in data analysis.
Replication	All experiments were repeated at least twice independently to ensure the replicability of the results. Independent biological replicates refer to the replication of the experiment with a different bacterial inoculum, infecting mice from a different litter, and processing the resulting samples independently from any other experiment.
Randomization	Mice were randomly assigned to each experimental group.
Blinding	For microscopy quantifications, observers were blinded to the experimental condition of the samples observed.

Reporting for specific materials, systems and methods

We require information from authors about some types of materials, experimental systems and methods used in many studies. Here, indicate whether each material, system or method listed is relevant to your study. If you are not sure if a list item applies to your research, read the appropriate section before selecting a response.

Materials & experimental systems

n/a	Involved in the study
☐	☒ Antibodies
☐	☒ Eukaryotic cell lines
☒	☐ Palaeontology and archaeology
☐	☒ Animals and other organisms
☒	☐ Human research participants
☒	☐ Clinical data
☒	☐ Dual use research of concern

Methods

n/a	Involved in the study
☒	☐ ChIP-seq
☐	☒ Flow cytometry
☒	☐ MRI-based neuroimaging

Antibodies

Antibodies used

Antibodies are described as : [Antigen recognized] [Fluorophore, if any] [catalog number] [provider] [dilution, if different from common dilution in each application] [URL to the provider webpage including validation data]

Flow Cytometry antibodies: Used at 1:300 unless stated otherwide

CD45 BV605 103139 BioLegend ; https://www.biolegend.com/en-us/products/brilliant-violet-605-anti-mouse-cd45-antibody-8721?GroupID=BLG6831

CD3 BV711 100241 BioLegend ; 1:100 ; https://www.biolegend.com/en-us/products/brilliant-violet-605-anti-mouse-cd45-antibody-8721?GroupID=BLG6831

CD3 FITC 100204 BioLegend ; 1:100 ; https://www.biolegend.com/en-us/products/fitc-anti-mouse-cd3-antibody-45

CD19 PE-Cy5 115510 BioLegend ; https://www.biolegend.com/en-us/products/pe-cyanine5-anti-mouse-cd19-antibody-1531

CD11b BUV737 564443 BD Biosciences ; https://www.bdbiosciences.com/en-fr/products/reagents/flow-cytometry-reagents/research-reagents/single-color-antibodies-ruo/buv737-rat-anti-cd11b.612800

CD11c BV785 117336 BioLegend; 1:100 ; https://www.biolegend.com/en-us/products/brilliant-violet-785-anti-mouse-cd11c-

antibody-7963?GroupID=BLG11937

Ly-6G PE-Cy7 127618 BioLegend ; https://www.biolegend.com/en-us/products/pe-cyanine7-anti-mouse-ly-6g-antibody-6139

Ly-6G APC-Cy7 127624 BioLegend ; https://www.biolegend.com/en-us/products/apc-cyanine7-anti-mouse-ly-6g-antibody-6755

Ly-6C PE 128008 BioLegend ; https://www.biolegend.com/en-us/products/pe-anti-mouse-ly-6c-antibody-4904

Ly-6C APC-Cy7 128026 BioLegend ; https://www.biolegend.com/en-us/products/apc-cyanine7-anti-mouse-ly-6c-antibody-6758

CD8a BUV395 563786 BD Biosciences ; https://www.bdbiosciences.com/en-fr/products/reagents/flow-cytometry-reagents/research-reagents/single-color-antibodies-ruo/buv395-rat-anti-mouse-cd8a.563786

CD8a PE-Dazzle594 100762 BioLegend ; https://www.biolegend.com/en-us/products/pe-dazzle-594-anti-mouse-cd8a-antibody-10069

CD69 PE-Cy7 104512 BioLegend ; https://www.biolegend.com/en-us/products/pe-cyanine7-anti-mouse-cd69-antibody-3168

CD4 PerCP-Cy5-5 100539 ; https://www.biolegend.com/en-us/products/percp-cyanine5-5-anti-mouse-cd4-antibody-4230

CD350 (NKp46) BV650 740627 BD Biosciences ; https://www.bdbiosciences.com/en-fr/products/reagents/flow-cytometry-reagents/research-reagents/single-color-antibodies-ruo/bv650-rat-anti-mouse-cd335-nkp46.740627

Fas/CD95 APC 152604 BioLegend ; 1:200; https://www.biolegend.com/en-us/products/apc-anti-mouse-cd95-fas-antibody-13906

LLO pentamer GYKDGNEYI PE 178 ProImmune ; 1:50; https://www.proimmune.com/

FLIP - 13250269 ThermoFisher ; 1:50; https://www.fishersci.fi/shop/products/anti-cflar-polyclonal-pa526132/13250269

Perforin PE 154306 BioLegend ; 1:200; https://www.biolegend.com/en-us/products/pe-anti-mouse-perforin-antibody-15255

Granzyme B Pacific blue 372218 BioLegend 1:200 ; https://www.biolegend.com/en-us/products/pacific-blue-anti-humanmouse-granzyme-b-recombinant-antibody-15596

CD127 BV421 135023 BioLegend 1:200 ; https://www.biolegend.com/en-us/products/brilliant-violet-421-anti-mouse-cd127-il-7ralpha-antibody-7193

IFNg BV711 505835 BioLegend ; 1:200; https://www.biolegend.com/en-us/products/brilliant-violet-711-anti-mouse-ifn-gamma-antibody-7950

KLRG1 PE 138408 BioLegend 1:200 ; https://www.biolegend.com/en-us/products/pe-anti-mouse-human-klrg1-mafa-antibody-6593

Cleaved caspase-3 biotinylated - 550557 BD Biosciences ; 1:100; https://www.bdbiosciences.com/en-fr/products/reagents/flow-cytometry-reagents/research-reagents/single-color-antibodies-ruo/biotin-rabbit-anti-active-caspase-3.550557

Ep-Cam APC-Cy7 118218 Biolegend ; 1:200; https://www.biolegend.com/en-us/products/apc-cyanine7-anti-mouse-cd326-ep-cam-antibody-5577

CD103 PE-Dazzle594 156909 Biolegend ; 1:200; https://www.biolegend.com/en-us/products/pedazzle-594-anti-mouse-cd103-recombinant-antibody-19823

CX3CR1 APC 149008 Biolegend ; 1:200; https://www.biolegend.com/en-us/products/apc-anti-mouse-cx3cr1-antibody-10460

IgG Rabbit-Alexa Fluor 700 A21038 ThermoFisher ; 1:250; https://www.fishersci.fi/shop/products/anti-rabbit-igg-h-l-alexa-fluor-700-conjugated-polyclonal-thermo-scientific-novex/

Microscopy : Antibodies used at 1:500 unless noted otherwise

CD11b - 550282 ThermoFisher 1:100 ; https://www.fishersci.fi/shop/products/cd11b-rat-anti-mouse-clone-m1-70-ebioscience-3/

Ly-6G - 551459 BD Biosciences 1:100 ; https://www.bdbiosciences.com/en-fr/products/reagents/flow-cytometry-reagents/research-reagents/single-color-antibodies-ruo/purified-rat-anti-mouse-ly-6g.551459

Ly-6C - Ab54223 Abcam 1:250 ; https://www.abcam.com/Ly6c-antibody-ER-MP20-ab54223.html

Listeria - 294562 Denka Seiken ; https://catalog.hardydiagnostics.com/cp_prod/Content/pdf/Antisera_Sellsheet.pdf

c-Met - AF527 R&DSystems 1:40 ; https://www.rndsystems.com/products/mouse-hgfr-c-met-antibody_af527

Phospho-Akt - 05-1003 Millipore ; https://www.merckmillipore.com/INTL/en/product/Anti-phospho-Akt-Ser473-Antibody-clone-6F5,MM_NF-05-1003

Gab-1 - sc-271848 Santa Cruz Biotechnology 1:100 ; https://www.scbt.com/p/gab-1-antibody-g-9

LAMP-1 - 553792 BD Pharmigen ; https://www.bdbiosciences.com/en-us/products/reagents/flow-cytometry-reagents/research-

reagents/single-color-antibodies-ruo/purified-rat-anti-mouse-cd107a.553792

CD8 - Ab22502 Abcam ; https://www.abcam.com/cd8-alpha-antibody-kt15-ab22502.html

GFP - Ab13970 Abcam 1:400 ; https://www.abcam.com/gfp-antibody-ab13970.html

IgG Rat-Alexa Fluor 488 A11006 ThermoFisher ; https://www.thermofisher.com/antibody/product/Goat-anti-Rat-IgG-H-L-Cross-Adsorbed-Secondary-Antibody-Polyclonal/A-11006

IgG Rabbit-Alexa Fluor 546 A11035 ThermoFisher ; https://www.thermofisher.com/antibody/product/Goat-anti-Rabbit-IgG-H-L-Highly-Cross-Adsorbed-Secondary-Antibody-Polyclonal/A-11035

IgG Chicken-Alexa Fluor 488 A11039 ThermoFisher ; https://www.thermofisher.com/antibody/product/Goat-anti-Chicken-IgY-H-L-Secondary-Antibody-Polyclonal/A-11039

IgG Goat-Alexa Fluor 546 A11056 ThermoFisher ; https://www.thermofisher.com/antibody/product/Donkey-anti-Goat-IgG-H-L-Cross-Adsorbed-Secondary-Antibody-Polyclonal/A-11056

IgG Rat-Alexa Fluor 647 A21247 ThermoFisher ; https://www.thermofisher.com/antibody/product/Goat-anti-Rat-IgG-H-L-Cross-Adsorbed-Secondary-Antibody-Polyclonal/A-21247

IgG Mouse-Alexa Fluor 647 A21463 ThermoFisher ; https://www.fishersci.fi/shop/products/anti-mouse-igg-h-l-alexa-fluor-647-conjugated-polyclonal-thermo-scientific-novex-2/

Western Blot antibodies :

InlB - Impens, F. et al. Nat. Microbiol. 2, 17005 (2017).
Ef-tu - Archambaud et al.Mol. Microbiol. 56, 383–396 (2005).
IgG Rabbit-Peroxidase - A6154 Sigma ; https://www.sigmaaldrich.com/FR/fr/product/sigma/a6154?gclid=Cj0KCQiA-qGNBhD3ARIsAO_o7ylTdBgi1dBkRF1dgWHdLImEaNp-8trzK7Tl4AeTUDBrhharScefXu0aAmllEALw_wcB

Validation

Commercial antibodies were validated on mouse tissues for either flow cytometry or microscopy by the producer, and URLs for each antibody validation data are provided in the box above. Other antibodies (anti InlB and anti EF-Tu) are validated in the referenced research article (see above).

Eukaryotic cell lines

Policy information about cell lines

Cell line source(s)	Vero cells (ATCC® CCL-81™)
Authentication	Cells were directly purchased from ATCC who performed authentication.
Mycoplasma contamination	All cells lines were negative for mycoplasma contamination
Commonly misidentified lines (See ICLAC register)	No commonly misidentified cell lines were used in this study.

Animals and other organisms

Policy information about studies involving animals; ARRIVE guidelines recommended for reporting animal research

Laboratory animals	Mice were housed in groups up to 7 animals, in BSL-3 animal facility, on Poplar chips (SAFE, D0736P00Z) and were fed with irradiated food at 25 kGy (SAFE, #150SP-25). The facility has central air conditioning equipment which maintains a constant temperature of 22± 2°C. Air is renewed at least 20 times per hour in animal rooms. Light is provided with a 14:10h light:dark cycle (6:30 a.m. to 8:30 p.m.). Animals were kept in polypropylene or polycarbonate cages which comply with European regulations in terms of floor surface per animal. All cages are covered with stainless steel grids and non-woven filter caps. 7-12 weeks-old mice were used, from strains : C57BL/6JRj ; BALB/c ; KIE16P , CX3CR1 GFP/+ ; iFABP-hEcad ; Rag2-/- ; CD3e-/- ; muMt-/-4; Ccr2-/- ; Rosa26-CreERT2 ; Rosa26-iDTR ; Faslpr-cg ; Prf1 KO ; Cflarflox/flox ; Metflox/flox ; LysM-CreERT2 Only female mice were used throughout the study, except for experiments involving FLIPflox/flox x LysMCreERT2 and Metflox/flox x LysMCreERT2 mice for which both male and female mice were included. Detailed informations about these strains can be found in the material and methods sections.
Wild animals	No wild animals were involved in the study.
Field-collected samples	No field collected samples were involved.
Ethics oversight	Animal experiments were performed according to the Institut Pasteur guidelines for laboratory animals' husbandry and in compliance with European regulation 2010/63 EU. All procedures were approved by the Animal Ethics Committee of Institut Pasteur, authorized by the French Ministry of Research and registered under #11995-201703115103592 and #14644-2018041116183944.

Flow Cytometry

Plots

Confirm that:

☒ The axis labels state the marker and fluorochrome used (e.g. CD4-FITC).

☒ The axis scales are clearly visible. Include numbers along axes only for bottom left plot of group (a 'group' is an analysis of identical markers).

☒ All plots are contour plots with outliers or pseudocolor plots.

☒ A numerical value for number of cells or percentage (with statistics) is provided.

Methodology

Sample preparation	Mice were euthanized at the indicated times post-infection. Functional characterization of CD8+ T cells and infected monocytes were performed after iv inoculation, unless stated otherwise, which allows for less intra-animal variation and thus reduces the number of animals needed for experiments. Counting and characterization of infected cells in the blood and spleen were performed at 4 days post-inoculation (both orally and iv), when bacteremia is the highest. For orally infected mice, the bacteremia being very low even at 4 days post-inoculation, blood of 3 mice was pooled and analyzed as one sample. Counting and characterization of infected cells in the intestine was performed after iv inoculation, to avoid early infection events linked to the inoculum passage of the intestinal barrier after oral inoculation, at 5 days post-inoculation, a time when the bacterial load is sufficient to detect late infection events. For cell death-related experiments and characterization of infected inflammatory monocytes, we harvested spleen at 3 dpi, the earliest timepoint at which the effect of InlB is consistently observed, but also when cell death is moderate in the spleen, so that we could harvest sufficient number of viable cells. Spleens, livers, mesenteric lymph nodes (MLN) and blood (by cardiac puncture in heparin-coated syringe) were harvested aseptically. Single cells suspensions were obtained from spleen and MLN by homogenizing through a 40 µm cell strainer. Single cells suspensions were obtained from liver using the Multi Tissue Dissociation Kit 1 (Miltenyi Biotec) and MACS apparatus (Miltenyi Biotec) following the manufacturer's instructions and successive filtration through 70 and 40 µm cell strainer. After red blood cells lysis using 1X RBC lysis buffer (eBiosciences), cells were washed in Cell Staining Buffer (CSB) (BioLegend) before further processing. Small intestines were harvested without conjunctive tissue, opened longitudinally, washed in ice-cold PBS and cut into 1-1.5 cm pieces and washed again in ice-cold PBS. Epithelial cells were first isolated after incubation of intestinal pieces in HBSS (Invitrogen) with 5% fetal calf serum, 10mM HEPES (Sigma) and 5mM EDTA for 3 times 20 min at 37°C with 200 rpm shaking. After washing in ice-cold DMEM (Invitrogen), leukocytes of the lamina propria were isolated after incubation in DMEM with DNase I (Roche) and Liberase TL (Roche) for 45 min at 37°C with 200 rpm shaking. Single cells suspensions of epithelial cells and leukocytes from the lamina propria were filtered successively through 100, 70 and 40 µm cell strainer, washed in ice-cold DMEM, then in CSB and processed further separately. If required, cells were labeled using the LiveBLAzerTM FRET-B/G Loading Kit with CCF2-AM (Invitrogen), a fluorescent substrate of beta-lactamase that can cross the plasma membrane. Presence of beta-lactamase-expressing bacteria in cells induces a shift in the fluorescence emission of the CCF2-AM substrate from 518 nM (green) to 447 nM (blue) upon excitation with the 405 nM laser and thus allows for identification of infected cells. Cells were loaded with the CCF2-AM substrate following manufacturer's instructions for 2h30 at room temperature in CSB containing 1mM probenecid (Sigma). After washing, cells were blocked using CD16/32 (BioLegend) for 5 min at room temperature, washed in CSB, stained with the appropriate antibodies (listed in Supplementary Information Table 6) for 45 min at 4°C and washed in CSB. If no intracellular staining was required, cells were suspended in CSB containing CountCAL beads (Sony) for absolute counting of cells. For intracellular staining, cells were fixed for 20 min at room temperature in IC fixation buffer (eBiosciences), washed three times in 1X permeabilization buffer (eBiosciences), incubated with primary antibodies for 1 hour at room temperature, washed and incubated with secondary antibodies for 45 min at room temperature. After washing, cells were suspended in CSB containing CountCAL beads for absolute counting of cells.
Instrument	Fortessa X-20 SORP apparatus (BD biosciences)
Software	FlowJo software v10 (TreeStar)
Cell population abundance	At least 100000 cells per mice were sorted using FACSAriaIII, at a flow rate below 5 (less that 20000 events/sec), in purity or single cells mode. Cells were plated and analyzed by microscopy to validate the sorting strategy.
Gating strategy	Debris were excluded from analysis based on their FSC-A SSC-A values. Doublets were excluded using FSC-AxFSC-W and SSC-AxSSC-W gating. Then cell populations were defined by gating on negative-positive signals, that were clearly distinct. The detailed gating strategies is presented in Supplementary Information Figure 2.

☒ Tick this box to confirm that a figure exemplifying the gating strategy is provided in the Supplementary Information.